Horst Köppel
David R. Yarkony
Heinz Barentzen
Editors

SPRINGER SERIES IN CHEMICAL PHYSICS 97

The Jahn-Teller Effect

Fundamentals and Implications for Physics and Chemistry

Springer

Horst Köppel
David R. Yarkony
Heinz Barentzen
(Eds.)

The Jahn-Teller Effect

Fundamentals and Implications for Physics and Chemistry

With 350 Figures

Springer

Professor Horst Köppel
Universität Heidelberg
Theoretische Chemie
Im Neuenheimer Feld 229
69120 Heidelberg
Germany
E-Mail: horst.koeppel@pci.uni-heidelberg.de

Professor Heinz Barentzen
MPI für Festkörperforschung
Heisenbergstr. 1
70569 Stuttgart
Germany
E-mail: h.barentzen@fkf.mpg.de

Professor David R. Yarkony
Johns Hopkins University
Department of Chemistry
3400 N. Charles Street
Baltimore MD 21218
USA
E-Mail: yarkony@jhu.edu

ISSN 0172-6218
ISBN 978-3-642-03431-2 e-ISBN 978-3-642-03432-9
DOI 10.1007/978-3-642-03432-9
Springer Heidelberg Dordrecht London New York

Library of Congress Control Number: 2009938946

Cover design: SPi Publisher Services

Printed on acid-free paper

Springer is part of Springer Science+Business Media (www.springer.com)

Preface

The Jahn–Teller (JT) effect continues to be a paradigm for structural instabilities and dynamical processes in molecules and in the condensed phase. While the basic theorem, first published in 1937, had to await experimental verification for 15 years, the intervening years saw rapid development, initially in the theoretical arena, followed increasingly by experimental work on molecules and crystals. The International Jahn–Teller Symposium was established in the mid-1970s, to foster the exchange of ideas between researchers in the field. Among the many important developments in the field, we mention cooperative phenomena in crystals, the general importance of pseudo-Jahn–Teller (PJT) couplings for symmetry-lowering phenomena in molecular systems, nonadiabatic processes at conical intersections of potential energy surfaces and extensions of the basic theory in relation to the discovery of fullerenes and other icosahedral systems.

It is the objective of this volume to provide the interested reader with a collection of tutorial reviews by leading researchers in the field. These reviews provide a comprehensive overview of the current status of the field, including important recent developments. This volume is targeted at both the non-expert scientist as well as the expert who wants to expand his/her knowledge in allied areas. It is intended to be a complement to the existing excellent textbooks in the field. Guided by the idea of tutorial reviews, we provide here short introductory remarks to the various sections, as they appear in the table of contents. These are followed by a brief characterization of the individual papers to make their basic contents, as well as their interrelation, more transparent.

1. Jahn–Teller Effect and Vibronic Interactions: General Theory

The first set of reviews deals with general formal aspects of the theory, its range of application and implementation. While the original formulation of the JT theorem applies to orbitally degenerate electronic states, it was later recognized that similar mechanisms for structural instabilities are operative also in nondegenerate states (PJT effect). In the first paper of this volume, Bersuker emphasizes the even more general implications of the JT and related couplings, by demonstrating that they may affect ground state structural properties, even when operative in the excited state manifold (hidden JT effect). This may be associated with spin-crossover effects and orbital disproportionation. The following two papers (by Ceulemans and Lijnen, and

by Breza) address group theoretical aspects. A desire has sometimes been expressed to gain more insight into the nature of the JT theorem than is afforded by the original proof (which consists in enumerating all topologically distinct realizations of all molecular point groups). This goal is indeed achieved in the article by Ceulemans and Lijnen. Poluyanov and Domcke advocate the use of the microscopic Breit-Pauli operator for the spin–orbit coupling rather than the phenomenological form often adopted. They point out that the resulting dependence of the spin–orbit coupling on the nuclear coordinates can lead to novel effects, of relevance to molecular spectra. Sato and coworkers present a scheme for analyzing vibronic coupling constants in terms of densities, which allows them to investigate their local properties and visualize their electronic origin. Finally, an efficient method to compute multimode JT coupling constants with density functional theory is presented by Zlatar et al. The approach uses information from the JT distorted structure, which is decomposed into contributions from the various relevant normal modes.

2. Conical Intersections and Nonadiabatic Dynamics in Molecular Processes

Conical intersections can be considered generalizations of the JT intersections in less symmetric cases, the latter being also conical in shape owing to the presence of the linear coupling terms predicted by the JT theorem. In molecular physics, conical intersections have emerged in the past one or two decades as paradigms for nonadiabatic excited-state dynamics, triggering a plethora of studies of elementary photophysical and photochemical processes. The article by Blancafort et al. reports on modern developments in the characterization of conical intersections by ab initio techniques. Their second-order analysis shows, for example, how to distinguish between minima and saddle points in the subspace of electronic degeneracy and to identify photochemically active coordinates. The paper by Bouakline et al. presents a quantum dynamical analysis of the smallest JT active system, triatomic hydrogen. This prototypical reactive scattering system is subject to geometric phase effects which, however, almost completely cancel out in the integral cross section. On the other hand, strong nonadiabatic couplings/geometric phase effects govern the upper-cone resonances (Rydberg states) of the system. The papers by Faraji et al. and by Reddy and Mahapatra present multimode quantum dynamical treatments of JT and PJT systems with more than two intersecting potential energy surfaces. Pronounced effects of the couplings in the spectral intensity distribution and in femtosecond (fs) internal conversion processes are identified. A systematic dependence of the phenomena on the (fluoro) substituents as well as the importance for the photostability of hydrocarbons is demonstrated. In the article by McKinlay and Paterson, similar phenomena, including nonadiabatic photodissociation processes and fs pump-probe spectroscopy, are discussed for transition metal complexes, thus providing a bridge between the JT effect and photochemistry.

3. Impurities; Spectroscopy of Transition Metal Complexes

Transition metal complexes have represented, for a long time, the archetypical system for which the JT effect plays a crucial role, especially with regard to crystal field splitting and spin–orbit interaction (Ham effect). This affects optical as well

as EPR spectra of 3d group ions, for example. In the review by Brik and Avram these are studied for various coordination sites using an effective Hamiltonian formalism. Useful relations for the Ham reduction factors are derived, and the JT parameters obtained from the Ham effect are compared with those obtained from the JT-distorted minima of the potential energy surfaces. Tregenna-Piggott and Riley present in their review a very pedagogic introduction to the Exe JT effect, and the Ham effect as one of its consequences. Applications to various types of spectra of different transition metal complexes underline the usefulness of the theoretical concepts. Garcia-Fernandez et al. address the question of structural instabilities of doped materials and their type and origin. They argue, and present convincing evidence, that these are frequently not due to differences in atomic sizes (as is often assumed in the literature) but rather to vibronic coupling, that is, the PJT effect. Finally in their review, Reinen and Atanasov analyze in their review, the effects of JT coupling on the changes from a high-spin to a low-spin electronic ground state in hexacoordinate fluoride complexes of Mn(III), Co(III), Ni(III) and Cu(III), an aspect which is frequently ignored in the literature on spin-crossover systems. In particular, the strong links to coordination and solid state chemistry are set out in this contribution.

4. Fullerenes and Fullerides

In the mid 1980s and subsequent years, the discovery of C_{60} and other fullerenes opened a route to the analysis of JT systems with higher than threefold degeneracies (G and H irreducible representations). This led to substantial developments from the point of view of pure theory as well as applications. This volume includes two important papers in this area. Structural aspects of fulleride salts, i.e. fullerene anions in various charge states in the solid state, are covered by Klupp and Kamaras. Evidence, based mostly on infrared spectroscopy, is used to discuss issues including static vs. dynamic JT effect, unusual phases, and relation to conductivity. The review by Hands et al. addresses the further complication of fullerenes being adsorbed on surfaces. The lowering in symmetry due to the surface interactions is considered, as well as the rather slow time-scale of the experimental technique of scanning tunneling microscopy proposed. Detailed simulations of the corresponding images shed useful light on their possible significance in establishing the presence and shape of JT distortions.

5. Jahn–Teller Effect and Molecular Magnetism

Molecular magnetism concerns the synthesis, characterization and application of molecular-based materials that possess the typical properties of magnets – slow relaxation, quantum tunneling and blocking of the magnetization at low temperatures (single molecular magnets (SMM)). It is an interdisciplinary research field which requires the combined efforts (cooperation) of chemists, molecular and solid state physicists, as well as theoreticians (quantum chemists). This is the point where the JT effect enters into the game. The magnetic properties of SMMs are affected by the structural influences caused by vibronic coupling and these influences are further manifested in the optical band shapes, the interactions between magnetic molecules

with degenerate ground states (cooperative JT effect), and the dynamical JT and PJT effects (which impact upon the magnetic relaxation and spin coherence times). In their review, Tsukerblat, Klokishner and Palii address these points in spin-frustrated systems with threefold symmetry, mixed valence systems, photoswitchable spin systems, and magnetic molecules which undergo tautomeric transformations leading to long-lived (metastable) states. The Jahn–Teller effect plays a crucial role in magnetic clusters built up from magnetic centers in orbitally degenerate ground states. Using a combination of ligand field theory and density functional theory Atanasov and Comba show how small structural changes due to Jahn–Teller activity and/or structural strains induce a dramatic lowering of the magnetic anisotropy. The same authors also show for the first time, using cyanide-bridged systems as model examples, how one can deduce the parameters of the spin Hamiltonian from first principles.

6. The Cooperative Jahn–Teller Effect and Orbital Ordering

It has long been recognized for JT crystals, i.e., crystals containing a JT center in each unit cell, that the intrinsic instability of JT complexes against distortions may give rise to an effective interaction between JT ions, mediated by the surrounding ligands of the ions. Below a critical temperature, this interaction may lead to the cooperative JT effect (CJTE), a structural phase transition where the whole crystal distorts. There are two main approaches to the CJTE, differing in the form of the effective ion–ion interaction. Kaplan's review is partly based on Kanamori's treatment, who generated this interaction by the transformation from local vibrational modes to phonons. This treatment, in combination with the canonical Hamiltonian shift transformation and a subsequent mean-field approximation, is the most popular approach to the CJTE. Although this concept, also referred to as virtual phonon exchange, has led to impressive results for some simpler systems, it cannot be applied to systems characterized by the Exe JT effect because of insurmountable technical difficulties. Such systems are conveniently treated by means of an alternative approach, developed by Thomas and co-workers and described in Polinger's article. This method assumes a bilinear lattice-dynamical interaction between the normal coordinates belonging to nearest-neighbor cells. However, the main emphasis of this article lies in a detailed comparison of the CJTE with the orbital-ordering (or Kugel-Khomskii) approach. A typical example of the orbital-ordering approach is presented in Ishihara's review. The main emphasis of this article is on the intrinsic orbital frustration effect, meaning that no orbital configuration exists, whereby the bond energies in all equivalent directions are simultaneously minimized. It is shown that the orbital frustration effect leads to several nontrivial phenomena in strongly correlated systems with orbital degrees of freedom. The influence of the CJTE and of JT impurities on material properties is elucidated in the reviews by Gudkov and Lucovsky. The review by Gudkov deals mainly with the influence of JT impurities on the elastic moduli and ultrasonic wave attenuation in diluted crystals. The elastic-wave technique broadens the facilities of JT spectroscopy in its low-energy part and provides new information, mostly about the properties of the ground state and its tunneling splitting. That the JT effect even plays an important role in semiconductor technology is convincingly demonstrated in Lucovsky's article. Here the CJTE

manifests itself in the group IVB transition-metal oxides, designed as replacement gate dielectrics for advanced metal-oxide-semiconductor devices.

7. Jahn–Teller Effect and High-Tc Superconductivity

The explanation of high-temperature superconductivity (HTSC) in copper oxides (cuprates) is one of the most difficult problems in modern physics. The undoped cuprates are antiferromagnetic Mott insulators, where the insulating behavior is caused by a strong on-site Coulomb repulsion. HTSC arises upon hole doping, whereupon the originally immobile electrons in the half-filled conduction band become mobile. The basic problem is to find the proper mechanism for the formation of Cooper pairs, the necessary ingredient of all superconductors. There are mainly two antagonistic views on the problem amounting to the question of whether the participation of phonons is indispensable for the pair formation or whether the electrons alone can do the job. The review by Miranda Mena tries to answer this question by gathering all available evidence in favor of electron–phonon mechanisms such as (bi)polarons and JT (bi)polarons. Seen in this perspective, the article gives a fair account of the state of the art in HTSCs. A more detailed theory of JT polarons and bipolarons with application to the fullerene superconductors is presented in the article by Hori and Takada. In addition to offering a thorough mathematical analysis, the authors also make the interesting observation that, for stronger coupling, JT polarons acquire a smaller effective mass than the Holstein polaron. Such a reduction of the polaron effective mass is essential for the existence of superconductivity, as the polaron mass increases with increasing coupling so that, for sufficiently strong coupling, the polaron becomes immobile and cannot contribute to the electric current. These remarks apply, in particular, to Koizumi's work, which proposes that the doped holes become small polarons and not, as is supposed in all electron-based theories of HTSC, constituents of Zhang-Rice singlets. As the mobility of the polarons is very limited, a novel mechanism is required to facilitate a macroscopic electric current. The author solves the problem by a loop current generation around each spin vortex due to the spin Berry phase. The macroscopic current is then the collection of all these loop currents.

This set of tutorial reviews has been created on the occasion of the 19th International Jahn–Teller Symposium, held in Heidelberg, University Campus, 25–29 August 2008. The volume does not, however, reflect directly the conference contents. Full coverage of the 46 oral presentations given at the meeting (plus a similar number of posters) was not attempted. Conversely, the 27 papers collected here go into considerably more depth than would be normal for a proceedings volume. We hope that this volume constitutes a valuable reference, for beginners and experts alike.

Heidelberg — *H. Köppel*
Stuttgart — *H. Barentzen*
Baltimore — *D.R. Yarkony*
May 2009

Acknowledgments

D. R. Yarkony acknowledges the support of NSF grant CHE-0513952. The editors are indebted to M. Atanasov for helpful comments.

Contents

List of Contributors

Stuart C. Althorpe Department of Chemistry, University of Cambridge, Cambridge CB2 1EW, UK

J.A. Aramburu Departamento de Ciencias de la Tierra y Física de la Materia Condensada, Universidad de Cantabria, 39005 Santander, Spain, antonio.aramburu@unican.es

Mihail Atanasov Institute of General and Inorganic Chemistry, Bulgarian Academy of Sciences, Acad.Georgi Bontchev Str., Bl.11, 1113 Sofia, Bulgaria, mihail.atanasov@aci.uni-heidelberg.de
and
Anorganisch-Chemisches Institut, Universität Heidelberg, Im Neuenheimer Feld 270, 69120 Heidelberg, Germany
and
Chemistry Department, Philipps-University, Hans-Meerwein-Strasse, 35043 Marburg, Germany

C.N. Avram Department of Physics, West University of Timisoara, Bvd.V. Parvan 4, Timisoara 300223, Romania

N.M. Avram Department of Physics, West University of Timisoara, Bvd. V. Parvan 4, Timisoara 300223, Romania
and
Academy of Romanian Scientists, Splaiul Independentei 54, 050094 Bucharest, Romania

M.T. Barriuso Departamento de Física Moderna, Universidad de Cantabria, 39005 Santander, Spain

Colin A. Bates School of Physics and Astronomy, University of Nottingham, Nottingham, NG7 2RD, UK

Michael J. Bearpark Department of Chemistry, Imperial College London, London SW7 2AZ, UK

Isaac B. Bersuker Institute for Theoretical Chemistry, The University of Texas at Austin, Austin, TX 78712, USA, bersuker@cm.utexas.edu

Lluís Blancafort Institut de Química Computacional and Parc Científic i Tecnològic, Universitat de Girona, 17071 Girona, Spain, lluis.blancafort@udg.edu

Foudhil Bouakline Department of Chemistry, University of Cambridge, Cambridge CB2 1EW, UK, foudhil.bouakline@googlemail.com

Martin Breza Department of Physical Chemistry, Slovak Technical University, 81237 Bratislava, Slovakia, martin.breza@stuba.sk

M.G. Brik Institute of Physics, University of Tartu, Riia Street 142, 51014 Tartu, Estonia

Arnout Ceulemans Department of Chemistry and INPAC Institute for Nanoscale Physics and Chemistry, Katholieke Universiteit Leuven, Celestijnenlaan 200F, 3001 Leuven, Belgium, Arnout.Ceulemans@chem.kuleuven.be

Peter Comba Anorganisch-Chemisches Institut, Universität Heidelberg, Im Neuenheimer Feld 270, 69120, Heidelberg, Germany, peter.comba@aci.uni-heidelberg.de

Claude Daul Department of Chemistry, University of Fribourg, Fribourg, Switzerland, claude.daul@unifr.ch

Wolfgang Domcke Department of Chemistry, Technische Universität München, 85747 Garching, Germany, wolfgang.domcke@ch.tum.de

Janette L. Dunn School of Physics and Astronomy, University of Nottingham, Nottingham, NG7 2RD, UK, Janette.Dunn@nottingham.ac.uk

Shirin Faraji Theoretische Chemie, Universität Heidelberg, Im Neuenheimer Feld 229, 69120 Heidelberg, Germany

P. García-Fernández Departamento de Ciencias de la Tierra y Física de la Materia Condensada, Universidad de Cantabria, 39005 Santander, Spain

J.M. García-Lastra Departamento de Física de Materiales, Facultad de Químicas, Universidad del País Vasco, 20018 San Sebastián, Spain

Etienne Gindensperger Laboratoire de Chimie Quantique, Institut de Chimie UMR 7177, CNRS/Université de Strasbourg, 4 rue Blaise Pascal, B.P. 1032, 67070 Strasbourg Cedex, France

Vladimir Gudkov Ural State Technical University, 19, Mira st., Ekaterinburg 620002, Russia, gudkov@imp.uran.ru

Ian D. Hands School of Physics and Astronomy, University of Nottingham, Nottingham, NG7 2RD, UK

Chishin Hori Institute for Solid State Physics, University of Tokyo, 5-1-5 Kashiwanoha, Kashiwa, Chiba 277-8581, Japan, chori@issp.u-tokyo.ac.jp

Sumio Ishihara Department of Physics, Tohoku University, Sendai 980-8578, Japan, ishihara@cmpt.phys.tohoku.ac.jp

Naoya Iwahara Department of Molecular Engineering, Graduate School of Engineering, Kyoto University, Nishikyo-ku, Kyoto 615-8510, Japan, iwaharanaoya@t03.mbox.media.kyoto-u.ac.jp

K. Kamarás Research Institute for Solid State Physics and Optics, Hungarian Academy of Sciences, Budapest, Hungary, kamaras@szfki.hu

Michael Kaplan Chemistry Department, Simmons College, 300 The Fenway, Boston, MA 02115, USA, michael.kaplan@simmons.edu
and
Physics Department, Simmons College, 300 The Fenway, Boston, MA 02115, USA

Sophia Klokishner Institute of Applied Physics of the Academy of Sciences of Moldova, Academy str. 5, Kishinev, 2028, Moldova

G. Klupp Research Institute for Solid State Physics and Optics, Hungarian Academy of Sciences, Budapest, Hungary, klupp@szfki.hu

Hiroyasu Koizumi Institute of Materials Science, University of Tsukuba, Tsukuba, Ibaraki 305-8573, Japan, koizumi@ims.tsukuba.ac.jp

Horst Köppel Theoretische Chemie, Universität Heidelberg, Im Neuenheimer Feld 229, 69120 Heidelberg, Germany, Horst.Koeppel@pci.uni-heidelberg.de

Aron Kuppermann Division of Chemistry and Chemical Engineering, California Institute of Technology, Pasadena, CA 91125, USA, aron@caltech.edu

Benjamin Lasorne CTMM, Institut Charles Gerhardt, UMR 5253, CC 1501, Université Montpellier II, 34095 Montpellier Cédex 5, France

Bruno Lepetit Université de Toulouse, UPS, Laboratoire Collisions Agrégats Réactivité, IRSAMC, 31062 Toulouse, France
and
CNRS, UMR 5589, 31062 Toulouse, France, bruno.lepetit@irsamc.ups-tlse.fr

Erwin Lijnen Department of Chemistry and INPAC Institute for Nanoscale Physics and Chemistry, Katholieke Universiteit Leuven, Celestijnenlaan 200F, 3001 Leuven, Belgium, Erwin.Lijnen@chem.kuleuven.be

Gerald Lucovsky Department of Physics, North Carolina State University, Raleigh, NC 27695-8202, USA, lucovsky@ncsu.edu

S. Mahapatra School of Chemistry, University of Hyderabad, Hyderabad-500046, India, smsc@uohyd.ernet.in

Russell G. McKinlay School of Engineering and Physical Sciences, Heriot-Watt University, Edinburgh, Scotland, EH14 4AS

Joaquin Miranda Mena Departamento de Física Aplicada, CINVESTAV-Mérida, Mérida, 97300, México, miranda.joaquin@gmail.com

M. Moreno Departamento de Ciencias de la Tierra y Física de la Materia Condensada, Universidad de Cantabria, 39005 Santander, Spain

Andrew Palii Institute of Applied Physics of the Academy of Sciences of Moldova, Academy str.5, Kishinev 2028, Moldova

Martin J. Paterson School of Engineering and Physical Sciences, Heriot-Watt University, Edinburgh, Scotland, EH14 4AS, m.j.paterson@hw.ac.uk

Victor Polinger Department of Chemistry, University of Washington, Seattle, WA 98195-17001, USA
and
Bellevue College, 3000 Landerholm Circle SE, Science Div., L-200, Bellevue, WA 98007, USA, polinv@u.washington.edu

Leonid V. Poluyanov Institute of Chemical Physics, Russian Academy of Sciences, Chernogolovka, Moscow 14232, Russian Federation

Catherine S.A. Rawlinson School of Physics and Astronomy, University of Nottingham, Nottingham, NG7 2RD, UK

D. Reinen Chemistry Department, Philipps-University, Hans-Meerwein-Strasse, 35043 Marburg, Germany, reinen@chemie.uni-marburg.de

Mark J. Riley School of Chemistry and Molecular Biosciences, University of Queensland, St. Lucia, QLD, 4072, Australia, m.riley@uq.edu.au

Michael A. Robb Department of Chemistry, Imperial College London, London SW7 2AZ, UK

Tohru Sato Fukui Institute for Fundamental Chemistry, Kyoto University, Kyoto, Japan
and
Department of Molecular Engineering, Graduate School of Engineering, Kyoto University, Nishikyo-ku, Kyoto 615-8510, Japan, tsato@scl.kyoto-u.ac.jp

Carl-Wilhelm Schläpfer Department of Chemistry, University of Fribourg, Fribourg, Switzerland, Carl-Wilhelm.Schlaepfer@unifr.ch

Katsuyuki Shizu Department of Molecular Engineering, Graduate School of Engineering, Kyoto University, Nishikyo-ku, Kyoto 615-8510, Japan, katsuyuki@21emon.mbox.media.kyoto-u.ac.jp

V. Sivaranjana Reddy School of Chemistry, University of Hyderabad, Hyderabad-500046, India, ch05ph07@uohyd.ernet.in

Yasutami Takada Institute for Solid State Physics, University of Tokyo, 5-1-5 Kashiwanoha, Kashiwa, Chiba 277-8581, Japan, takada@issp.u-tokyo.ac.jp

Kazuyoshi Tanaka Department of Molecular Engineering, Graduate School of Engineering, Kyoto University, Nishikyo-ku, Kyoto 615-8510, Japan, a51053@sakura.kudpc.kyoto-u.ac.jp

Ken Tokunaga Research and Development Center for Higher Education, Kyushu University, Ropponmatsu, Fukuoka 810-8560, Japan, tokunaga@rche.kyushu-u.ac.jp

Philip L.W. Tregenna-Piggott Laboratory for Neutron Scattering, ETH Zürich and Paul Scherrer Institut, CH-5232 Villigen PSI, Switzerland, philip.tregenna@psi.ch

A. Trueba Departamento de Ciencias de la Tierra y Física de la Materia Condensada, Universidad de Cantabria, 39005 Santander, Spain

Boris Tsukerblat Department of Chemistry, Ben-Gurion University of the Negev, PO Box 653, 84105 Beer-Sheva, Israel, tsuker@bgu.ac.il

Graham A. Worth School of Chemistry, University of Birmingham, Egbaston, Birmingham B15 2TT, UK

Matija Zlatar Department of Chemistry, University of Fribourg, Fribourg, Switzerland
and
Center for Chemistry, IHTM, University of Belgrade, Belgrade, Serbia, matija.zlatar@unifr.ch,matijaz@chem.bg.ac.rs

Polarons and Bipolarons in Jahn–Teller Crystals

Chishin Hori and Yasutami Takada

Abstract A review is made on the developments in the last two decades in the field of the Jahn–Teller effect on itinerant electrons in Jahn–Teller crystals. Special attention is paid to the current status of the researches on the fullerene superconductors and the manganite perovskites exhibiting the colossal magnetoresistance. Present knowledge about the polarons and bipolarons in the typical Jahn–Teller model systems is also summarized, together with some original results of our own.

1 Introduction

Physics and chemistry of the Jahn–Teller (JT) effect started from the theory in 1930s [1], investigating structural instabilities of high-symmetry configurations in molecules. The theory has been developed further and sophisticated in the next several decades to provide a very general quantum-mechanical framework for treating a particular type of electron-vibrational (or electron–phonon) coupling in molecules or solids in which two or more orbitally degenerate (or pseudodegenerate) electronic states are mixed nonadiabatically through ionic (or lattice) vibrational modes.

Due to its intrinsic complexity arising from the orbital multiplicity, the researches in this field have been almost exclusively concerned with the JT effect in rather simple systems like molecules, small clusters, and a single JT impurity center in solids in which itinerant electrons do not play an important role [2,3]. Even if the JT crystals, in which an infinite number of such JT centers occupy regular positions in a lattice, are considered in the context of the cooperative JT effect, relevant electrons in the system have usually been assumed to be localized [4].

A surge of a new sort of interest in the JT effect occurred in the late 1980s when high-temperature superconductivity (HTSC) was discovered in the copper oxides [5]. Because these compounds may be regarded as a class of the JT crystals, people began to pay much attention to *the JT effect on itinerant electrons*. In 1990s the interest in the JT effect in metals was intensified by both the discovery of superconductivity in the alkali-metal-doped fullerides of the type A_3C_{60} with A = K, Rb, Cs (or their combinations) [6] and the subsequent one of the colossal magnetoresistance (CMR) in the manganite perovskites [7,8].

As for the current status of the researches on these materials, a rather comprehensive review was given by Bersuker in Sect. 8.4 of [3] from the standpoint of elucidating the roles of the JT effect. Therefore it would not be necessary to reiterate a similar kind of review here, particularly for the issue of HTSC for which Bersuker made a very detailed account, but it might be appropriate for us to make some supplementary comments or remarks on the issues of the CMR and the fullerene superconductors from our perspective that is reflecting the experience of one of the authors (Y.T.) who was engaged in the studies on those issues in 1990s.

The CMR is a technical term to indicate the phenomenon of a strong variation of the electric resistance with the change of applied magnetic fields, as observed, for example, in $La_{1-x}Ca_xMnO_3$ with x in the range between 0.2 and 0.4. The conduction electrons in these compounds are composed of the Mn e_g orbitals with the density of $1-x$ electrons per Mn ion, implying that the system can be regarded as a JT crystal of the canonical $E \otimes e$ type. It is widely believed that the double-exchange (DE) mechanism associated with the Hund's-rule coupling between the Mn t_{2g} localized core spins and the mobile e_g electrons [9–11] plays a crucial role in making a qualitatively correct explanation of the CMR, but an important claim was made that the JT coupling was also needed for its quantitatively accurate description [12]. This claim has been confirmed by both experiment using the state-of-the-art photospectroscopy [13] and theory based on the first-principles calculation of the electronic band structure and the electron–phonon coupling constant [14, 15]. Thus the CMR can be regarded as the outcome of the interplay among spin, charge, orbital, and phonon degrees of freedom, as emphasized in several review articles on the manganites [16–22].

This complicated interplay has made the physics of manganites very rich and we can enumerate several fascinating proposals of new physics in relation to these compounds, including (1) *the cooperative JT effect mediated by electron hopping* rather than by phonons (or lattice distortions) [14], (2) *the phase-separation scenario* for the CMR in the manganites, in which the Coulomb correlation is considered to be a more important competitor with the DE mechanism than the electron–phonon coupling [17], (3) *the concept of the complex-orbital ordering*, in which linear superposition of basic orbitals, $d_{x^2-y^2}$ and $d_{3z^2-r^2}$, with complex coefficients is suggested [23], (4) *the topological-phase scenario* for the formation of the stripe and the charge-ordered states, in which the key notion is the winding number (the Chern integers) associated with the Berry-phase connection of an e_g electron parallel transported through the JT centers along zigzag one-dimensional paths in an antiferromagnetic environment of the t_{2g} core spins [24, 25], and (5) *the concept of the geometric energy* which is defined as the difference in energy caused by the change in the winding number [26]. This is a concept proposed in analogy to the exchange energy (or the spin singlet-triplet energy splitting) in the case of spin degrees of freedom.

This complication in the manganites, however, has also a negative side, because it obscures the actual role of the JT effect on the CMR. In fact, what is actually confirmed so far is that the conduction electron should not be treated as a bare band electron but a rather small polaron in order to obtain the CMR in the experimentally

observed magnitude, if we try to explain the CMR in terms of a one-conduction-electron picture. This polaron motion can be realized not only through the $E \otimes e$ coupling (or *the off-diagonal vibrational coupling* in degenerate electronic-state representation) but also through the conventional Holstein model [27] in which a nondegenerate electronic orbital (A) is coupled to a nondegenerate non-JT phonon (a), leading to the "$A \otimes a$" problem with *the diagonal vibrational coupling*. In this respect, we do not know to what extent the JT effect is an indispensable factor in bringing about the CMR. In order to give a definite answer to this question, we need to know, first of all, more detailed information about the similarities and the differences in the polaronic nature between the $E \otimes e$ JT and the $A \otimes a$ Holstein models. Section 3 of this article addresses this issue by comparing the results of the one-electron problem in various theoretical models, each of which is described by the Hamiltonian introduced in Sect. 2.

The fulleride is an insulating molecular crystal in which narrow threefold conduction bands (with the bandwidth W of the order of 0.5 eV) are derived from the triply-degenerate t_{1u} LUMO orbitals of a C_{60} molecule. With the doping of three alkali atoms per one C_{60}, we obtain the metallic compound A_3C_{60} in which the conduction bands are half-filled. This compound exhibits superconductivity with the transition temperature T_c over 30K and the short coherence length ξ_0 of only a few times the C_{60}-C_{60} separation. The conduction electron interacts with various intramolecular phonons (two nondegenerate a_g modes and eight fivefold degenerate h_g multiplets), but the high-energy ($\omega_0 \approx 0.2$ eV) tangential h_g modes couple most strongly to the electron, as suggested by the first-principles calculations [28–31], implying that A_3C_{60} can be modeled as a JT crystal of the $T_{1u} \otimes h_g$ type.

As discussed in many review articles [32–39], superconductivity in A_3C_{60} is generally understood in terms of a simple BCS picture of the s-wave pairing driven by these high-energy h_g intramolecular JT phonons. This understanding is based on, among others, the observation of the isotope effect on T_c by the substitution of ^{13}C for ^{12}C [40–43] and also on the reproduction of the observed T_c by using the McMillan's formula [44, 45]

$$T_c = \frac{\omega_0}{1.2} \exp\left[-\frac{1.04(1+\lambda)}{\lambda - \mu^*(1+0.62\lambda)}\right], \tag{1}$$

in which the nondimensional electron–phonon coupling constant λ is evaluated to be in the range $0.5 - 1$ [28–30] and the Coulomb pseudopotential μ^* is taken as about 0.2. In particular, the characteristic dependence of T_c on the lattice constant of the crystal a_0 is well reproduced in this BCS scenario [46].

A closer look at this system, however, reveals that the present situation is not so clear and simple. In fact, it is far from being settled for the reasons given in the following: (1) The McMillan's formula is derived based on the Migdal–Eliashberg (ME) theory for superconductivity [47] which is valid only when the parameter ω_0/E_F (with E_F the Fermi energy) is small enough to neglect the vertex corrections [48]. In A_3C_{60}, however, this parameter is not small, owing to the fact that $E_F (\approx W/2)$ is about the same as ω_0. Thus we need to consider the contribution

from the vertex corrections [49]. (2) In the case of $E_F \approx \omega_0$, the concept of μ^* is not applicable, either [50], requiring that the electron–electron and electron–phonon interactions should be treated on an equal footing. Actually, the Coulomb repulsion between electrons U (or the Coulomb correlation) is strong in the C_{60} molecule, rendering the interplay of this repulsion including the Hund's-rule coupling J with the phonon-mediated attraction $-U_{ph}$ as a matter of intense research even in a single-site $T_{1u} \otimes h_g$ JT system [51–55]. (3) As mentioned before, the isotope effect for the completely substituted $A_3{}^{13}C_{60}$ can be explained quantitatively well with resort to the McMillan's formula, but it is concluded [56] that the formula can never explain the intriguing experiment done by Chen and Lieber who observed the large difference in T_c between the atomically substituted $Rb_3(^{13}C_x{}^{12}C_{1-x})_{60}$ and the molecularly substituted $Rb_3(^{13}C_{60})_x(^{12}C_{60})_{1-x}$ [57,58].

In order to overcome these difficulties, Han, Gunnarsson, and Crespi have calculated the on-site pairing susceptibility in the dynamical mean-field theory (DMFT) [59] and claimed that the JT phonons in both $E \otimes e$ and $T_{1u} \otimes h_g$ systems bring about a local (intramolecular) Cooper pair which does not suffer much from the effect of large U, in contrast to the non-JT phonons in the Holstein ($A \otimes a$) model [60]. They have also claimed that with the change of the parameters such as U, λ, and the conduction-electron density n, the obtained T_c behaves much differently from that predicted in the McMillan formula (or in the ME theory), leading to a qualitative explanation of the interesting T_c versus n dependence as observed in $Na_2Cs_xC_{60}$ and $K_{3-x}Ba_xC_{60}$ compounds [61]. These interesting results, however, are still open to debate, partly because the effect of the Hund's-rule coupling J is not considered in their work, though it is evident that J works to destroy the intramolecular (or on-site) Cooper pair, and partly because there is a completely opposite claim that the ME theory is very robust in the JT systems [62,63].

In relation to the Hund's-rule coupling J, there is another controversial claim that the dynamical feature of the JT phonons is not crucial at all in such a strongly-correlated system as A_3C_{60}, especially in the situation near the Mott–Hubbard transition [64,65] or the antiferromagnetic (AF) state [66]. According to their claim, the only role that the JT phonons can play is to make J effectively negative, leading to the multi-band Hubbard model with the on-site strong repulsion U and an additional inverted Hund's-rule coupling, based on which superconductivity in the fullerides is addressed [67,68].

A further simplification of the system is pursued by arguing that even the band-multiplicity is not crucial, either, as long as the physical parameters are chosen appropriately. What really matters is only *the strong competition between the phonon-mediated attraction $-U_{ph}$ and the local Coulomb repulsion U*. Actually, by adopting the Hubbard–Holstein model (or the $A \otimes a$ system with the on-site Coulomb repulsion U) and exploiting the fact that the coherence length ξ_0 is very short [70], the calculations of T_c have been done, with the electron–electron and electron–phonon interactions treated on an equal footing, to find that the experimental results, including (a) the relations between T_c and a_0 in both fcc and simple cubic lattices [36,69], (b) the experiment by Chen and Lieber on the anomalous isotope effect [57,71], and (c) the relation between T_c and n [36,61], are all successfully

reproduced in a coherent fashion. The point here is the consideration of the off-site pairing (leading to the extended s-wave nature) composed of not the bare electrons but the (phonon fully-dressed) polarons in order to avoid the strong on-site repulsion [72].

To summarize, much more works, with taking various aspects into account, are needed to obtain a full understanding of the mechanism of superconductivity in A_3C_{60}. Even in the $E \otimes e$ and $T_{1u} \otimes h_g$ model systems, setting aside the fullerides, the JT effect on superconductivity, especially in the presence of the Coulomb effect including the Hund's-rule coupling, is not known well. To some extent we shall address this issue in the model JT systems in Sect. 4 of this article.

Incidentally, in any kind of the strong-coupling electron–phonon systems, there is always a subtle argument on the competition between the two scenarios for the occurrence of superconductivity; one for the formation of a Cooper pair of two polarons and the other for bipolaron superconductivity [73–78]. In the former, the pair formation and superconductivity occur simultaneously, while in the latter, the bipolaron is formed first and then its Bose-Einstein condensation (BEC) brings about superconductivity. At the present stage of the theoretical investigations in this field, there is no precise knowledge about the conditions to make the one scenario dominate the other, but it is usually presumed that the second scenario will apply, if the electron–phonon coupling λ is large enough. Therefore we shall be mainly concerned with this situation and treat the bipolaron formation and its BEC in Sect. 4. In the rest of this article, we shall employ units in which $k_B = \hbar = 1$.

2 Preliminaries

2.1 *Models for JT Crystals*

Let us imagine a lattice composed of N JT centers at which electronic and phononic states are, respectively, N_e- and n_{ph}-fold degenerate. In general, we may decompose the Hamiltonian H for this system as

$$H = \sum_{\mathbf{j}} H_{\mathbf{j}} + H_t + H_{\text{elastic}} + H_V, \tag{2}$$

where $H_{\mathbf{j}}$ is the part containing all the possible terms defined at site $\mathbf{j}$, H_t describes the inter-site hoppings of electrons, H_{elastic} represents the elastic interactions between neighboring sites (or the inter-site phonon–phonon interactions), and H_V takes care of the inter-site Coulomb repulsions. In the fullerides, we need not consider H_{elastic} from the outset and H_V will not be crucial. In the manganites, on the other hand, H_{elastic} may be important [14] and H_V may also be important in considering the nanoscale phase separation, but because we are not primarily concerned with either the cooperative JT effect mediated by phonons or the phase-separation scenario, we shall forget both H_{elastic} and H_V altogether in this article.

With the assumption that electrons hop only between nearest-neighbor sites, we may write H_t in second quantization as

$$H_t = -\sum_{(\mathbf{j},\mathbf{j}')} \sum_{\gamma,\gamma'=1}^{N_e} \sum_{\sigma} t_{\mathbf{j}\mathbf{j}'}^{\gamma\gamma'} \left(c_{\mathbf{j}\gamma\sigma}^{\dagger} c_{\mathbf{j}'\gamma'\sigma} + c_{\mathbf{j}'\gamma'\sigma}^{\dagger} c_{\mathbf{j}\gamma\sigma} \right), \tag{3}$$

where $t_{\mathbf{j}\mathbf{j}'}^{\gamma\gamma'}$ is the overlap integral between the electron orbital γ at site $\mathbf{j}$ and the other γ' at site $\mathbf{j}'$ and $c_{\mathbf{j}\gamma\sigma}^{\dagger}$ ($c_{\mathbf{j}\gamma\sigma}$) creates (annihilates) an electron at site $\mathbf{j}$ with orbital $\gamma(=1,\ldots,N_e)$ and spin $\sigma(=\uparrow,\downarrow)$. The actual values for $t_{\mathbf{j}\mathbf{j}'}^{\gamma\gamma'}$ can be determined in a concrete manner [25], once the crystal structure is specified, but if we are not concerned with some specific situation, we shall take

$$t_{\mathbf{j}\mathbf{j}'}^{\gamma\gamma'} = \begin{cases} t & \text{for a nearest-neighbor pair } \langle \mathbf{j},\mathbf{j}' \rangle \text{ and } \gamma = \gamma', \\ 0 & \text{otherwise,} \end{cases} \tag{4}$$

which is the simplest choice for this hopping matrix.

The site term $H_{\mathbf{j}}$ consists of the chemical-potential term $H_{\mathrm{c}}^{(\mathbf{j})}$, the electron–electron interaction term $H_{\mathrm{cc}}^{(\mathbf{j})}$, the phononic term $H_{\mathrm{ph}}^{(\mathbf{j})}$, and the electron–phonon coupling term $H_{\mathrm{e-ph}}^{(\mathbf{j})}$. (The coupling with the t_{2g} core spins is needed in the manganites, but it is neglected here.) The first and second terms are written as

$$H_{\mathrm{c}}^{(\mathbf{j})} = -\mu \sum_{\gamma\sigma} n_{\mathbf{j}\gamma\sigma}, \tag{5}$$

$$\begin{aligned} H_{\mathrm{cc}}^{(\mathbf{j})} =& U \sum_{\gamma} n_{\mathbf{j}\gamma\uparrow} n_{\mathbf{j}\gamma\downarrow} + \frac{1}{2} U' \sum_{\gamma\neq\gamma'} \sum_{\sigma\sigma'} n_{\mathbf{j}\gamma\sigma} n_{\mathbf{j}\gamma'\sigma'} \\ &+ \frac{1}{2} J \sum_{\gamma\neq\gamma'} \sum_{\sigma\sigma'} c_{\mathbf{j}\gamma\sigma}^{\dagger} c_{\mathbf{j}\gamma'\sigma'}^{\dagger} c_{\mathbf{j}\gamma\sigma'} c_{\mathbf{j}\gamma'\sigma} + \frac{1}{2} J' \sum_{\gamma\neq\gamma'} \sum_{\sigma} c_{\mathbf{j}\gamma\sigma}^{\dagger} c_{\mathbf{j}\gamma-\sigma}^{\dagger} c_{\mathbf{j}\gamma'-\sigma} c_{\mathbf{j}\gamma'\sigma}, \end{aligned} \tag{6}$$

where μ is the chemical potential and $n_{\mathbf{j}\gamma\sigma}(= c_{\mathbf{j}\gamma\sigma}^{\dagger} c_{\mathbf{j}\gamma\sigma})$ denotes the electron number operator. The on-site Coulomb interaction is prescribed by the parameters U, U', J, and J', which represent, respectively, the magnitudes of the intra-orbital repulsive, the inter-orbital repulsive, the orbital-exchange (or the Hund's-rule coupling), and the pair-exchange interactions. These parameters are related to each other through

$$U = U' + J + J' = U' + 2J. \tag{7}$$

In (7), rotational symmetry in the degenerate-orbital space leads to the first equality, while we can derive the second one (or $J = J'$) by comparing the concrete analytical expressions for J and J' [20].

With use of the phonon energy ω_0, the phononic term is given simply as

$$H_{\mathrm{ph}}^{(\mathrm{j})} = \omega_0 \sum_{\nu=1}^{n_{ph}} a_{\mathrm{j}\nu}^{\dagger} a_{\mathrm{j}\nu}, \tag{8}$$

with $a_{\mathrm{j}\nu}^{\dagger}$ ($a_{\mathrm{j}\nu}$) the local-phonon creation (annihilation) operator at site j with mode $\nu(= 1, \ldots, n_{ph})$. Finally, the coupling term $H_{\mathrm{e-ph}}^{(\mathrm{j})}$ is described as

$$H_{\mathrm{e-ph}}^{(\mathrm{j})} = g_{N_e \otimes n_{ph}} \sum_{\nu} \sum_{\gamma\gamma'} \sum_{\sigma} V_{\gamma\gamma'}^{(\nu)} c_{\mathrm{j}\gamma\sigma}^{\dagger} c_{\mathrm{j}\gamma'\sigma} (a_{\mathrm{j}\nu} + a_{\mathrm{j}\nu}^{\dagger}), \tag{9}$$

where $g_{N_e \otimes n_{ph}}$ is the electron–phonon coupling constant characterizing the $N_e \otimes n_{ph}$ JT center and $V_{\gamma\gamma'}^{(\nu)}$ is its coupling matrix element. Its concrete form will depend on the type of the JT system. For example, in the $E \otimes e$ system in which the electronic orbitals are $d_{x^2-y^2}$ and $d_{3z^2-r^2}$ for $\gamma = 1(= \epsilon)$ and $2(= \theta)$, respectively, the results for $V^{(\nu)} \equiv (V_{\gamma\gamma'}^{(\nu)})$ with $\nu = 1(= \epsilon)$ and $2(= \theta)$ are written as

$$V^{(1)} = \begin{pmatrix} 0 & 1 \\ 1 & 0 \end{pmatrix} \text{ and } V^{(2)} = \begin{pmatrix} 1 & 0 \\ 0 & -1 \end{pmatrix}. \tag{10}$$

In the $T \otimes t$ system, on the other hand, they are given as

$$V^{(1)} = \begin{pmatrix} 0 & 0 & 0 \\ 0 & 0 & 1 \\ 0 & 1 & 0 \end{pmatrix}, V^{(2)} = \begin{pmatrix} 0 & 0 & 1 \\ 0 & 0 & 0 \\ 1 & 0 & 0 \end{pmatrix}, \text{and } V^{(3)} = \begin{pmatrix} 0 & 1 & 0 \\ 1 & 0 & 0 \\ 0 & 0 & 0 \end{pmatrix}, \tag{11}$$

while in the $T \otimes h$ system, they are obtained as

$$V^{(1)} = \frac{\sqrt{3}}{2} \begin{pmatrix} 0 & 0 & 0 \\ 0 & 0 & 1 \\ 0 & 1 & 0 \end{pmatrix}, V^{(2)} = \frac{\sqrt{3}}{2} \begin{pmatrix} 0 & 0 & 1 \\ 0 & 0 & 0 \\ 1 & 0 & 0 \end{pmatrix}, V^{(3)} = \frac{\sqrt{3}}{2} \begin{pmatrix} 0 & 1 & 0 \\ 1 & 0 & 0 \\ 0 & 0 & 0 \end{pmatrix},$$

$$V^{(4)} = \frac{\sqrt{3}}{2} \begin{pmatrix} 1 & 0 & 0 \\ 0 & -1 & 0 \\ 0 & 0 & 0 \end{pmatrix}, \text{and } V^{(5)} = \frac{1}{2} \begin{pmatrix} -1 & 0 & 0 \\ 0 & -1 & 0 \\ 0 & 0 & 2 \end{pmatrix}. \tag{12}$$

Of course, $V^{(1)} = 1$ for the $A \otimes a$ system.

In considering electron motion in a crystal, it is convenient to introduce momentum representation which is the Fourier transform of site representation as

$$c_{\mathrm{k}\gamma\sigma} = \frac{1}{\sqrt{N}} \sum_{\mathrm{j}} e^{-i\mathrm{j}\cdot\mathrm{k}} c_{\mathrm{j}\gamma\sigma} \text{ and } a_{\mathrm{k}\nu} = \frac{1}{\sqrt{N}} \sum_{\mathrm{j}} e^{-i\mathrm{j}\cdot\mathrm{k}} a_{\mathrm{j}\nu}. \tag{13}$$

In this representation, H_t can be diagonalized. In particular, under the assumption of (4), we obtain

$$H_t + \sum_{\mathrm{j}} H_{\mathrm{c}}^{(\mathrm{j})} = \sum_{\mathrm{k}\gamma\sigma} (\epsilon_{\mathrm{k}} - \mu)\, c_{\mathrm{k}\gamma\sigma}^{\dagger} c_{\mathrm{k}\gamma\sigma}, \tag{14}$$

with ϵ_{k} the single-electron dispersion relation, which is given by

$$\epsilon_{\mathrm{k}} = -2t \sum_{i=1}^{d} \cos k_i, \tag{15}$$

for a simple cubic lattice in d dimensions. Though the results will not be given here, other parts of the Hamiltonian can be rewritten accordingly in this representation.

2.2 *Conservation of Pseudospin Angular Momentum*

In the $E \otimes e$ JT system, we can define T_{j} the operator to rotate *pseudospin* at site j by

$$T_{\mathrm{j}} = \mathrm{i}\left(a_{\mathrm{j}\epsilon}^{\dagger} a_{\mathrm{j}\theta} - a_{\mathrm{j}\theta}^{\dagger} a_{\mathrm{j}\epsilon}\right) - \frac{\mathrm{i}}{2} \sum_{\sigma} \left(c_{\mathrm{j}\epsilon\sigma}^{\dagger} c_{\mathrm{j}\theta\sigma} - c_{\mathrm{j}\theta\sigma}^{\dagger} c_{\mathrm{j}\epsilon\sigma}\right). \tag{16}$$

As easily checked, this operator commutes with H_{j}, leading to the local conservation law of "pseudospin angular momentum" in the electron–phonon coupled system. If (4) is assumed, the total pseudospin rotation operator $T(\equiv \sum_{\mathrm{j}} T_{\mathrm{j}})$ is conserved in the entire crystal.

In order to better exploit this local conservation law, we shall change the representation in which the one-body basis functions are the eigen functions of both the Hamiltonian and T_{j}. This can be accomplished by the following canonical transformation from the basis functions (ϵ, θ) to those (α, β) as

$$\begin{pmatrix} d_{\mathrm{j}\alpha\sigma} \\ d_{\mathrm{j}\beta\sigma} \end{pmatrix} = \frac{1}{\sqrt{2}} \begin{pmatrix} 1 & -\mathrm{i} \\ 1 & \mathrm{i} \end{pmatrix} \begin{pmatrix} c_{\mathrm{j}\epsilon\sigma} \\ c_{\mathrm{j}\theta\sigma} \end{pmatrix} \text{ and } \begin{pmatrix} b_{\mathrm{j}\alpha} \\ b_{\mathrm{j}\beta} \end{pmatrix} = \frac{1}{\sqrt{2}} \begin{pmatrix} -\mathrm{i} & 1 \\ \mathrm{i} & 1 \end{pmatrix} \begin{pmatrix} a_{\mathrm{j}\epsilon} \\ a_{\mathrm{j}\theta} \end{pmatrix}. \tag{17}$$

In this new representation, $H_{\mathrm{c-ph}}^{(\mathrm{j})}$ and T_{j} are, respectively, rewritten as

$$H_{\mathrm{c-ph}}^{(\mathrm{j})} = \sqrt{2} g_{E\otimes e} \sum_{\sigma} \left[\left(b_{\mathrm{j}\alpha} + b_{\mathrm{j}\beta}^{\dagger}\right) d_{\mathrm{j}\alpha\sigma}^{\dagger} d_{\mathrm{j}\beta\sigma} + \left(b_{\mathrm{j}\alpha}^{\dagger} + b_{\mathrm{j}\beta}\right) d_{\mathrm{j}\beta\sigma}^{\dagger} d_{\mathrm{j}\alpha\sigma}\right], \tag{18}$$

$$T_{\mathrm{j}} = b_{\mathrm{j}\alpha}^{\dagger} b_{\mathrm{j}\alpha} - b_{\mathrm{j}\beta}^{\dagger} b_{\mathrm{j}\beta} + \frac{1}{2} \sum_{\sigma} \left(d_{\mathrm{j}\alpha\sigma}^{\dagger} d_{\mathrm{j}\alpha\sigma} - d_{\mathrm{j}\beta\sigma}^{\dagger} d_{\mathrm{j}\beta\sigma}\right). \tag{19}$$

Equation (18) for $H_{\mathrm{e-ph}}^{(\mathrm{j})}$ explicitly expresses the characteristic feature of *the off-diagonal electron–phonon coupling*, in contrast to the *the diagonal electron–phonon coupling* in the $A \otimes a$ Holstein model [27], in which $H_{\mathrm{e-ph}}^{(\mathrm{j})}$ is described as

$$H_{\mathrm{e-ph}}^{(\mathrm{j})} = g_{A\otimes a} \sum_{\sigma} \left(a_{\mathrm{j}}^{\dagger} + a_{\mathrm{j}} \right) c_{\mathrm{j}\sigma}^{\dagger} c_{\mathrm{j}\sigma}. \tag{20}$$

The existence of the conserved pseudospin rotation is not a common feature among the JT systems. In fact, we cannot define an operator corresponding to T_{j} in both $T \otimes t$ and $T \otimes h$ systems. Mathematical analysis of the continuous group invariances in each JT system determines the presence/absence of such an operator [79]; the $SO(2)$ invariance in the $E \otimes e$ system generates the operator T_{j}, while there are no such invariances in the $T \otimes t$ system. In Sect. 3, we shall find an unexpected consequence of this mathematical structure of the JT system in the behavior of the polaron mass.

2.3 *Theoretical Tools*

There are various theoretical tools to investigate the polaron and bipolaron problems. In the weak-coupling region, the standard method is the perturbation-theoretic approach including the Green's-function method. In the strong-coupling region, on the other hand, the canonical transformation due to Lang and Firsov [80] is commonly used. This is a method very similar to the Lee–Low–Pines unitary transformation [81] developed for the Fröhlich model [82] and provides a very useful trial wavefunction for many types of variational approaches.

These are basically analytic methods, but in recent years numerical methods play a major role. Among them, the simplest one is exact diagonalization in which the Hamiltonian matrix obtained with an appropriate expansion basis is numerically diagonalized. This is very elementary, but due to the bosonic character of phonons, the size of the Hamiltonian matrix increases exponentially as N and/or N_e increase. Thus it is not easy to treat the $E \otimes e$ system with more than two sites by this method.

In order to take care of larger systems, more sophisticated methods have been employed. For example, path-integral quantum Monte Calro (PIQMC) [83] is a powerful method in which bosonic degrees of freedom are analytically integrated out to provide an effective self-interaction working on an electron and the remaining integral is performed through quantum Monte Carlo (QMC) simulations. Since the polaron problem does not suffer from the notorious negative-sign problem, we can hope to obtain accurate results for a lattice of very large N and arbitrary dimensions by using QMC. Other advanced methods include; (1) density-matrix renormalization group (DMRG) [84], (2) the large-scale variational method called "variational exact diagonalization (VED)" [85,86], (3) dynamical Mean-field theory (DMFT) [87], and (4) diagrammatic Monte Carlo (DMC) [88]. It is very fortunate that useful textbooks on these methods have recently been published [89, 90]. We suggest interested readers to consult them for details.

3 Polaron: Single-Electron Problem

In the polaron problem (or the single-electron system coupled with phonons), both spin degrees of freedom and the electron–electron interaction as described by $H_{cc}^{(j)}$ are irrelevant. The first work on the JT polaron was done by Höck et al. [91] on the $E \otimes b$ system [92] which, unfortunately, possesses a too simple internal structure to provide qualitatively different features from those of the $A \otimes a$ system. Several works have treated the second simplest $E \otimes e$ system and found a quantitative difference in the polaron effective mass from that in the $A \otimes a$ system [63,93–98]. The $T \otimes t$ JT polaron has also been studied and the difference from that in the $E \otimes e$ system is revealed [99–101].

Let us start with the $E \otimes e$ JT polaron in the weak-coupling region (or for the case of small $g_{E\otimes e}$), in which the perturbation approach in momentum representation is useful. The thermal one-electron Green's function $G_{\mathbf{k}\gamma\sigma}(i\omega_n)$ with ω_n the fermion Matsubara frequency is defined at temperature T by

$$G_{\mathbf{k}\gamma\sigma}(i\omega_n) = -\int_0^{1/T} d\tau\, e^{i\omega_n\tau}\langle T_\tau d_{\mathbf{k}\gamma\sigma}(\tau) d_{\mathbf{k}\gamma\sigma}^\dagger\rangle. \tag{21}$$

This function is related to the self-energy $\Sigma_{\mathbf{k}\gamma\sigma}(i\omega_n)$ through the Dyson equation as $G_{\mathbf{k}\gamma\sigma}(i\omega_n)^{-1} = i\omega_n - \epsilon_{\mathbf{k}} + \mu - \Sigma_{\mathbf{k}\gamma\sigma}(i\omega_n)$. In Fig. 1, diagrammatic representation for $\Sigma_{\mathbf{k}\gamma\sigma}(i\omega_n)$ are given, together with the formal expansion series for the vertex function $\Gamma_{\gamma'\sigma',\gamma\sigma}(\mathbf{k}'i\omega_{n'}, \mathbf{k}i\omega_n)$. Using the self-energy analytically continued on the real frequency axis, we can determine the polaron (renormalized) dispersion relation $E_{\mathbf{k}}$ by the solution of $E_{\mathbf{k}} = \epsilon_{\mathbf{k}} + \Sigma_{\mathbf{k}\gamma\sigma}(E_{\mathbf{k}}) - \mu$. The bare band mass m and the polaron effective mass m^* are derived from the curvatures of $\epsilon_{\mathbf{k}}$ and $E_{\mathbf{k}}$ at $\mathbf{k} = \mathbf{0}$, respectively. Of course, the polaron stabilization energy $E_{\mathrm{JT}}(\approx -g_{E\otimes e}^2/\omega_0)$ is obtained as the shift of $\mu(= -E_{\mathrm{JT}})$.

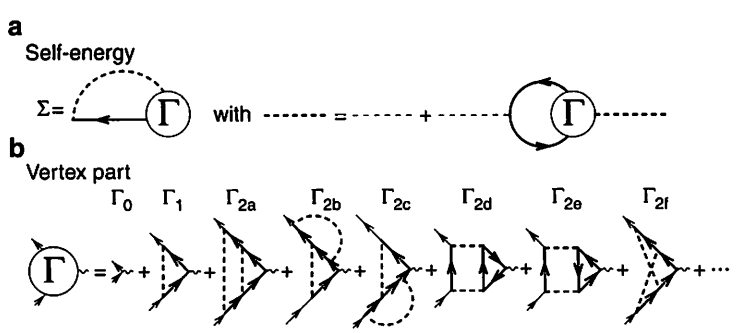

Fig. 1 (**a**) Self-energy in diagrammatic representation. (**b**) Expansion series for the vertex Γ up to g^4. *Thick solid, thick dashed, and thin dashed lines* indicate, respectively, the electron Green's function, the dressed phonon, and the bare phonon propagators

In the weak-coupling region, we may replace $G_{\mathbf{k}\gamma\sigma}(i\omega_n)$ by the bare one $(i\omega_n - \epsilon_{\mathbf{k}} + \mu)^{-1}$ in Fig. 1 and take $\Gamma_{\gamma'\sigma',\gamma\sigma}(\mathbf{k}'i\omega_{n'}, \mathbf{k}i\omega_n)$ as unity or the first term Γ_0 in Fig. 1b. Then we obtain the result for the mass ratio m^*/m, the most fundamental quantity in the polaron physics, as

$$\frac{m^*}{m} = 1 + 2\left(\frac{g_{E\otimes e}}{\omega_0}\right)^2. \tag{22}$$

Similar calculations can be done for $A \otimes a$, $T \otimes t$, and $T \otimes h$ to find

$$\frac{m^*}{m} = 1 + \left(\frac{g_{A\otimes a}}{\omega_0}\right)^2, \frac{m^*}{m} = 1 + 2\left(\frac{g_{T\otimes t}}{\omega_0}\right)^2, \text{and} \frac{m^*}{m} = 1 + \frac{5}{3}\left(\frac{g_{T\otimes h}}{\omega_0}\right)^2, \tag{23}$$

from which we see that it is exactly the same mass enhancement factor in all the cases, if we normalize the coupling constants in the following way:

$$g_{A\otimes a} = g, g_{E\otimes e} = \frac{1}{\sqrt{2}}g, g_{T\otimes t} = \frac{1}{\sqrt{2}}g, \text{ and } g_{T\otimes h} = \sqrt{\frac{3}{5}}g. \tag{24}$$

In fact, there is no qualitative difference between the JT polaron and the Holstein polaron in this region. Even quantitatively, they are exactly the same, as long as the coupling constants are normalized according to (24).

In the strong-coupling limit, a polaron will be completely localized at a single site, indicating $m^*/m = \infty$, and the problem is reduced to *a single-site system* in which the polaron stabilization energy is a main issue [102]. For a finite but very large coupling, the localized polaron will begin to hop between sites, but the hopping in this case is a very rare event. Thus physics connected with such a hopping can be well captured by just considering *a two-site system*. The same is true for the anti-adiabatic case in which t is very small, implying that the hopping is a very rare event from the outset.

Now, we need to know a formula to evaluate m^*/m from the eigen-state energies in a finite-site system. For this purpose, let us consider a one-dimensional ($d = 1$) infinite chain first. By making an expansion of the bare dispersion ϵ_k in (15) around $k = 0$, we see that $t = 1/2m = [\max\{\epsilon_k\} - \min\{\epsilon_k\}]/4$, where $\max/\min\{\epsilon_k\}$ is the maximum/minimum value of ϵ_k in the entire Brillouin zone. With the introduction of the electron–phonon interaction, t will be modified effectively into t^*. Then we can follow a similar argument to reach the relation of $t^* = 1/2m^* = [\max\{E_k\} - \min\{E_k\}]/4$. By taking the ratio of these results, we obtain an interesting result as $m^*/m = [\max\{\epsilon_k\} - \min\{\epsilon_k\}]/[\max\{E_k\} - \min\{E_k\}]$. In this derivation, we have assumed one dimensionality, but exactly the same result can be obtained even if we consider in both 2D and 3D, indicating that m^*/m can be evaluated only through the polaron bandwidth, $\max\{E_k\} - \min\{E_k\}$, irrespective of dimensionality.

The total polaron bandwidth can be estimated by calculating E_k in finite-site systems where some discrete values of k's are available. In the two-site problem, if we write the ground-state wavefunction for a polaron localized at site $\mathbf{j}$ as $\Psi_{\mathbf{j}}$, the

ground- and the first-excited-state wavefunctions in a two-site (j = 1 or 2) system are well represented by $\Psi_+ = (\Psi_1 + \Psi_2)/\sqrt{2}$ and $\Psi_- = (\Psi_1 - \Psi_2)/\sqrt{2}$, respectively, in the region under consideration. The former corresponds to the bonding state ($k = 0$) with energy E_+ and the latter to the anti-bonding one ($k = \pi$) with energy E_-. Then, since $\epsilon_\pi - \epsilon_0 = 2t$ in the two-site calculation, we obtain m^*/m through the relation

$$\frac{m^*}{m} = \frac{2t}{E_- - E_+}. \tag{25}$$

Note that the result m^*/m obtained through (25) does not depend on the value t in the strong-coupling and/or anti-adiabatic region.

With use of (25), a rigorous analytical result has already been obtained for the $E \otimes e$ JT polaron as [93]

$$\frac{m^*}{m} = I_0(g^2_{E\otimes e}/\omega_0^2) + I_1(g^2_{E\otimes e}/\omega_0^2) \approx \frac{2}{\sqrt{\pi}}\frac{\omega_0}{g}\exp\left[\frac{1}{2}\left(\frac{g}{\omega_0}\right)^2\right], \tag{26}$$

where $I_i(x)$ is the modified Bessel function of ith order and (24) is used in arriving at the last equation. Compared to $m^*/m = \exp[(g/\omega_0)^2]$ the Holstein's famous factor for the $A \otimes a$ system, we come to realize that m^*/m becomes much less enhanced in the $E \otimes e$ polaron than that in the Holstein model.

By comparing the result of m^*/m for the infinite-site system obtained by VED [96] (see, Fig. 2), we are confident that the two-site calculation provides a reasonably good result for m^*/m in the whole range of g at least in the anti-adiabatic region of t/ω_0. The relevance of the two-site calculation has also been seen in the Holstein model [78]. Thus we can expect that the same is true for the $T \otimes t$ JT polaron. In Fig. 3, we show the result of m/m^* for the $T \otimes t$ system (*solid curve*) which is obtained in the anti-adiabatic region by implementing an

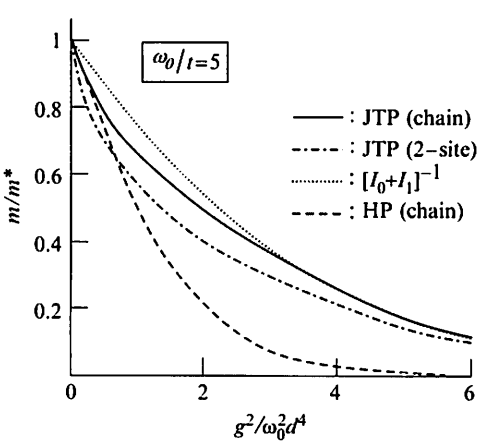

Fig. 2 Inverse of the polaron mass enhancement factor, m/m^*, as a function of g^2/ω_0^2 for the $A \otimes a$ (HP: Holstein polaron) and the $E \otimes e$ JT polaron. In the latter, the result in the infinite chain ($d = 1$) is compared with that in the two-site system as well as the analytic result in (26). The anti-adiabatic condition of $\omega_0/t = 5$ is assumed

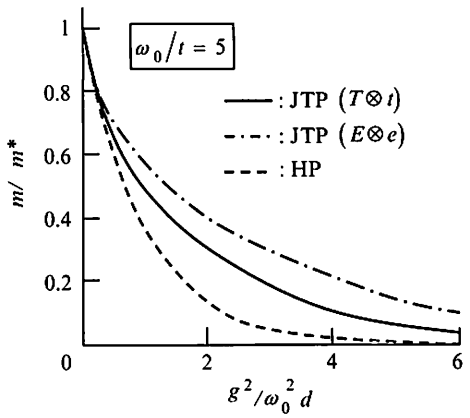

Fig. 3 Inverse of the mass enhancement factor, m/m^*, as a function of g^2/ω_0^2 with $d = 1$ for the $T \otimes t$ (*solid curve*) and the $E \otimes e$ (*dotted-dashed curve*) JT polarons in comparison with the Holstein one (*dashed curve*). All the results are obtained by exact diagonalization applied to the two-site Hamiltonian in the anti-adiabatic region

exact diagonalization study of the two-site Hamiltonian [100, 101]. This result is situated between the corresponding ones for the $E \otimes e$ JT (*dotted-dashed curve*) and the $A \otimes a$ Holstein (*dashed curve*) polarons.

Physically the polaron mass enhancement is brought about by the virtual excitation of phonons. In the $A \otimes a$ Holstein model no restriction is imposed on exciting multiple phonons, implying that all the terms in Fig. 1b for the vertex function contribute, while in the $E \otimes e$ JT model, there is a severe restriction due to the existence of the conservation law intimately related to the $SO(2)$ rotational symmetry in the pseudospin space. Actually, among the first- and second-order terms for the vertex function, only the term Γ_{2f} contributes, leading to the smaller polaron mass enhancement factor m^*/m than that in the Holstein model in which the correction Γ_1 is known to enhances m^*/m very much. In this way, the applicable range of the Migdal's approximation [48] becomes much wider in the $E \otimes e$ JT system [63].

In order to understand the reason why the result for m^*/m in the $T \otimes t$ JT system comes between those in the $A \otimes a$ and $E \otimes e$ systems, we shall rewrite $H_{\mathrm{c-ph}}^{(\mathrm{j})}$ in (9) for the $T \otimes t$ system as [101]

$$
\begin{aligned}
H_{\mathrm{c-ph}}^{(\mathrm{j})} = \sqrt{\frac{2}{3}}\, g_{T\otimes t}\Big[& (b_{\mathrm{j}1}^{+} + b_{\mathrm{j}2})(d_{\mathrm{j}1\sigma}^{+} d_{\mathrm{j}3\sigma} + d_{\mathrm{j}3\sigma}^{+} d_{\mathrm{j}2\sigma} - 2d_{\mathrm{j}2\sigma}^{+} d_{\mathrm{j}1\sigma}) \\
& + (b_{\mathrm{j}1} + b_{\mathrm{j}2}^{+})(d_{\mathrm{j}3\sigma}^{+} d_{\mathrm{j}1\sigma} + d_{\mathrm{j}2\sigma}^{+} d_{\mathrm{j}3\sigma} - 2d_{\mathrm{j}1\sigma}^{+} d_{\mathrm{j}2\sigma}) \\
& + (b_{\mathrm{j}3}^{+} + b_{\mathrm{j}3})(2d_{\mathrm{j}3\sigma}^{+} d_{\mathrm{j}3\sigma} - d_{\mathrm{j}1\sigma}^{+} d_{\mathrm{j}1\sigma} - d_{\mathrm{j}2\sigma}^{+} d_{\mathrm{j}2\sigma})\Big],
\end{aligned}
\tag{27}
$$

by introducing an appropriate unitary transformation. The first two terms in (27) has a structure very similar to that in (18) representing the feature of *the off-diagonal electron–phonon coupling*, which makes many terms in the vertex correction vanish. On the other hand, the last term in (27) has the feature of *the diagonal electron–phonon coupling* as in the $A \otimes a$ system. In this respect, the system $T \otimes t$ may be regarded as $T \otimes (a \oplus e)$, an intermediate character.

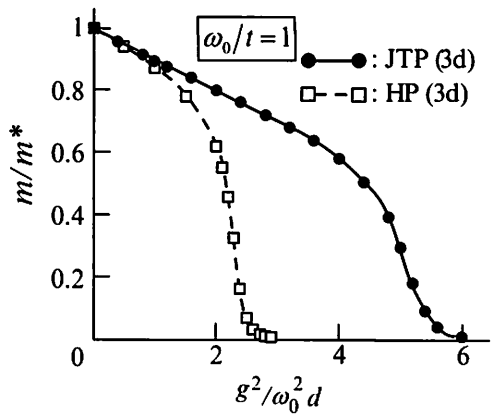

Fig. 4 Inverse of the mass enhancement factor, m/m^*, for the $E \otimes e$ JT polaron as a function of $g^2/3\omega_0^2$ in the simple cubic lattice, in comparison with the corresponding result in the Holstein polaron [94]

The reduction of $t \rightarrow a \oplus e$ can also be ascertained by considering the adiabatic potential energy surface for the $T \otimes t$ system. The potential contains four equivalent wells for sufficiently large $g_{T\otimes t}$ [103–105], but the wells are not isotropic and the vibrational t-mode splits into an a-mode of energy ω_0 and two e-modes of energy $\sqrt{2/3}\,\omega_0$.

In Fig. 4, m/m^* for the $E\otimes e$ JT polaron in the intermediate-adiabaticity region is given in comparison with the corresponding one for the Holstein polaron in the simple cubic lattice ($d = 3$). The results are obtained by PIQMC [94] and the physical message is just the same as the one we have already explained.

In concluding this section, we emphasize an amazing fact that the internal mathematical structure of the JT center determines the magnitude of the polaron effective mass. This implies that there will be an intrinsic difference in m^* between the manganese oxides $La_{1-x}Sr_xMnO_3$ with e_g electrons and the titanium ones $La_{1-x}Sr_xTiO_3$ with t_{2g} electrons, as may be observed by the difference in the transport mass or the T-linear coefficient in the low-temperature electronic specific heat $C_v(T)$ [101]. The experimental result on $C_v(T)$ obtained by Tokura's group [106] may be relevant to this issue.

4 Bipolarons: Problems with Two or More Electrons

4.1 Bipolaron Formation

If there are two or more electrons in the system, we should take the Coulomb correlation into account by considering $H_{ee}^{(j)}$ given in (6). In the case of the $E \otimes e$ system, using (7) and (17), we can rewrite (6) into

$$H_{\mathrm{ee}}^{(\mathrm{j})} = (U' + J)\sum_{\gamma} n_{\mathrm{j}\gamma\uparrow} n_{\mathrm{j}\gamma\downarrow} + (U' + J)\sum_{\sigma} n_{\mathrm{j}\alpha\sigma} n_{\mathrm{j}\beta-\sigma}$$
$$+ (U' - J)\sum_{\sigma} n_{\mathrm{j}\alpha\sigma} n_{\mathrm{j}\beta\sigma} + 2J\sum_{\sigma} d_{\mathrm{j}\alpha\sigma}^{\dagger} d_{\mathrm{j}\beta-\sigma}^{\dagger} d_{\mathrm{j}\alpha-\sigma} d_{\mathrm{j}\beta\sigma}$$
$$= \frac{\bar{U}}{2} n_{\mathrm{j}} (n_{\mathrm{j}} - 1) - 2J\sum_{\sigma} n_{\mathrm{j}\alpha\sigma} n_{\mathrm{j}\beta\sigma} + 2J\sum_{\sigma} d_{\mathrm{j}\alpha\sigma}^{\dagger} d_{\mathrm{j}\beta-\sigma}^{\dagger} d_{\mathrm{j}\alpha-\sigma} d_{\mathrm{j}\beta\sigma}, \quad (28)$$

where $\bar{U} \equiv U' + J$ and $n_{\mathrm{j}} \equiv \sum_{\gamma\sigma} n_{\mathrm{j}\gamma\sigma}$.

In addition to the Coulomb interaction, the phonon-mediated interactions U_{ph} work on the electrons. In the weak-coupling and anti-adiabatic region, the lowest-order perturbation calculation provides $U_{\mathrm{ph}} = \sum_{\mathrm{j}} U_{\mathrm{ph}}^{(\mathrm{j})}$ with $U_{\mathrm{ph}}^{(\mathrm{j})}$ obtained as

$$U_{\mathrm{ph}}^{(\mathrm{j})} = 2\frac{g_{E\otimes e}^2}{\omega_0}\sum_{\sigma} n_{\mathrm{j}\alpha\sigma} n_{\mathrm{j}\beta\sigma} - 2\frac{g_{E\otimes e}^2}{\omega_0}\sum_{\sigma} d_{\mathrm{j}\alpha\sigma}^{\dagger} d_{\mathrm{j}\beta-\sigma}^{\dagger} d_{\mathrm{j}\alpha-\sigma} d_{\mathrm{j}\beta\sigma}, \quad (29)$$

in the $E \otimes e$ system. By comparing (29) with (28), we notice that the phonon-exchange effect makes J decrease, while $\bar{U}$ unchanged at least up to this order of perturbation. This result is somewhat different from the one in the single-band system. In fact, in the case of the $A \otimes a$ system with the Hubbard-U interaction $H_U (= U\sum_{\mathrm{j}} n_{\mathrm{j}\uparrow} n_{\mathrm{j}\downarrow})$, the corresponding U_{ph} is obtained as

$$U_{\mathrm{ph}} = -2\frac{g_{A\otimes a}^2}{\omega_0}\sum_{\mathrm{j}} n_{\mathrm{j}\uparrow} n_{\mathrm{j}\downarrow}, \quad (30)$$

indicating that the Coulomb repulsion U itself is reduced by the phonon-induced attraction. Of course, the electron–phonon interaction shifts both the hopping integral t and the chemical potential μ as well.

The formation of a bipolaron (or a bound pair of two polarons) is established, if the ground-state energy of the two-electron system is lower than twice the ground-state energy of a polaron. This issue has been studied rather intensively for the Holstein bipolaron [78], but it is not the case for the JT bipolaron. In [96], the electron–electron correlation function and the effective mass of an $E \otimes e$ bipolaron was studied in one dimension in comparison with the corresponding results for the Holstein bipolaron [107]. In Fig. 5, we plot the phase diagram for the bipolaron formation, from which we find that the JT bipolaron is less stable than the Holstein one.

4.2 *Two-Site Four-Electron $E \otimes e$ System*

Due to huge dimensions of the Hilbert space for JT systems, it is quite difficult to treat many JT polarons even with state-of-the-art supercomputers. Therefore we

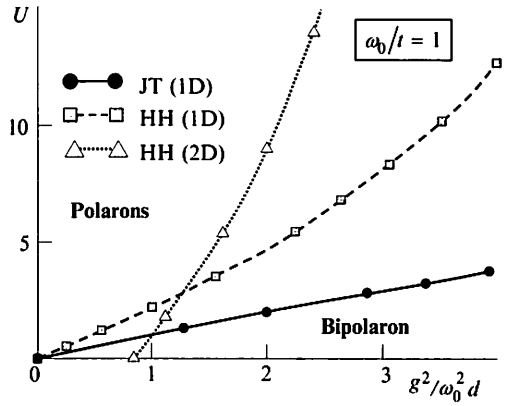

Fig. 5 Phase boundary for the bipolaron formation [96, 107]. The spatial dimension of the system is indicated by d

have to be satisfied with studying small clusters, if we resort to exact diagonalization or its marginal refinements.

Here we present our results of the two-site $E \otimes e$ JT model at half-filling (two electrons per site on average) at which the competition between the Coulomb repulsion and the JT-phonon induced attraction becomes very eminent, because both the Hund's-rule coupling and the pair-exchange interaction work only if two electrons exist at the same site. This two-site calculation is of particular relevance to the physics of a crystal in the anti-adiabatic and/or strong-coupling region, but we may claim that studying this system is generally the first and important step towards a full understanding of the physics connected with the electron hopping effect in JT crystals due to the fact that a two-site system is a minimal model containing electron hopping terms in the presence of various kinds of competing interactions.

As a work preceding to ours, Han and Gunnarsson [108] treated three kinds of one- and two-site JT models ($E \otimes a$, $E \otimes e$, and $T \otimes h$) in considering the metal-insulator transition (MIT) in A_nC_{60} with $n = 3$ or 4. They were mainly concerned with the parameters in the region of

$$g \ll \omega_0 \ll W \ll U \text{ and } J \sim g^2/\omega_0 \ll W, \tag{31}$$

in which the effects of the Hund's-rule and the JT couplings manifest themselves as merely first- and second-order perturbation, respectively. Here W denotes the bare bandwidth. Then, as mentioned before, the effect of the JT coupling simply cancels that of the exchange integral J, excluding more subtle physics driven by the competition of the JT and Hund's-rule couplings. We shall discuss this subtle physics by relaxing the parameter space from the conditions specified in (31).

Before discussing the calculated results, let us consider the two limiting cases first. One is the limit of $g(= \sqrt{2}g_{E\otimes e}) \to \infty$, in which four electrons form two bipolarons with each localized at a different site due to the fact that the $E \otimes e$ coupling favors the spin-singlet electron pair per site. The structure of the electronic wave function corresponding to this situation is shown schematically in Fig. 6. Due

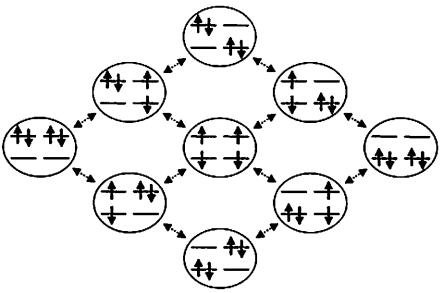

Fig. 6 Structure of the electronic wave function for the two-site $E \otimes e$ system at half-filling. This structure schematically represents "the intra-site singlet state". *Double-sided arrows* indicate the connection of the matrix elements of the wave function via the $E \otimes e$ coupling

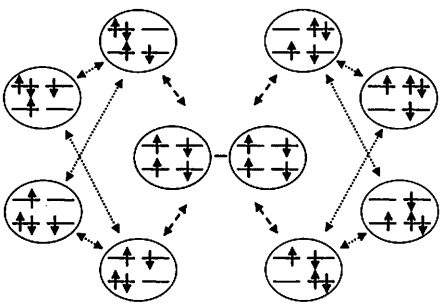

Fig. 7 Similar schematic view of the Structure of the electronic wave function for the two-site $E \otimes e$ system at half-filling. This structure represents the state dominated by "the inter-site singlet state". In this case, double-sided arrows indicate the connection of the matrix elements of the wave function via both the $E \otimes e$ coupling and the usual inter-site hopping

to large g, the effective hopping amplitude t^* is virtually zero, making the system insulating. In particular, in the limit of $g \to \infty$, the ground state is characterized by *an orbital ordering*. In the intermediate-coupling region, however, it can be an insulator without the orbital ordering or *a nonmagnetic JT Mott insulator*, as suggested by Fabrizio and Tosatti [109]. The detail of the orbital ordering depends on the choice of $t_{ij}^{\gamma\gamma'}$: In the diagonal hopping ($t_{ij}^{\gamma\gamma'} = t\delta_{\gamma\gamma'}$), an antiferro-orbital (AFO) ordering is more favorable than a ferro-orbital one.

Another limit is to take $J \to \infty$ with keeping U'/J fixed.[1] Due to large U' and J, each site is occupied by two electrons with parallel spins, but the total spin of the ground state S is not two but zero owing to the superexchange interaction, suggesting an antiferromagnetic or a spin density wave (SDW) state the structure of which is schematically shown in Fig. 7.

[1] In view of the fact that U' and J are, more or less, of the same order of magnitude in actual materials, we consider this condition to be reasonable.

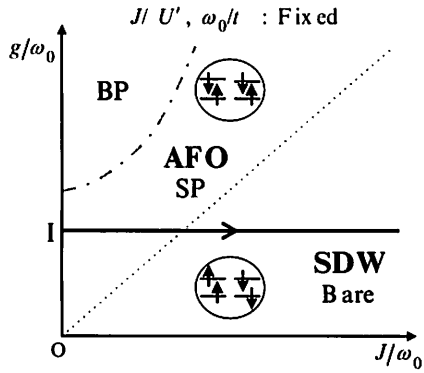

Fig. 8 Schematic phase diagram for the two-site $E \otimes e$ system at half-filling in the (g, J) space. AFO and SDW indicate, respectively, antiferro-orbital ordering and spin density wave states. The electronic state is specified by either the bare electron (Bare), the single-polaron (SP), or the bipolaron (BP). Parameters g, ω_0/t, and J/U' are, respectively, chosen as 1, 1, 0.5 along the line I

In Fig. 8, a schematic phase diagram is shown to connect the above two limits by changing the parameters g and J. We shall focus our attention on the intermediate-coupling region along the line I in this figure, where a strong competition between g and J is expected. This competition is investigated by the calculation of various physical quantities with use of exact diagonalization. Along the line I, the parameters g, ω_0/t, and J/U' are set equal to be 1, 1, 0.5, respectively. These values are chosen in reference to the manganites.

The calculated quantities include charge density wave (CDW), spin density wave, antiferro-orbital ordering, and electron-pairing response functions. The corresponding operators are the density operator A^{c}, the spin density operator A^{s}, the antiferro-orbital operator A^{o}, and the singlet pairing operator Φ, all of which are defined in terms of the original orbitals of $\epsilon(= d_{x^2-y^2})$ and $\theta(= d_{3z^2-r^2})$ as

$$A^{\mathrm{c}} = \frac{1}{2}\sum_{\gamma\sigma}\left(c^{\dagger}_{1\gamma\sigma}c_{1\gamma\sigma} - c^{\dagger}_{2\gamma\sigma}c_{2\gamma\sigma}\right), \tag{32}$$

$$A^{\mathrm{s}} = \frac{1}{2}\sum_{\gamma}\left[\left(c^{\dagger}_{1\gamma\uparrow}c_{1\gamma\uparrow} - c^{\dagger}_{1\gamma\downarrow}c_{1\gamma\downarrow}\right) - \left(c^{\dagger}_{2\gamma\uparrow}c_{2\gamma\uparrow} - c^{\dagger}_{2\gamma\downarrow}c_{2\gamma\downarrow}\right)\right], \tag{33}$$

$$A^{\mathrm{o}} = \frac{1}{2}\sum_{\sigma}\left[\left(c^{\dagger}_{1\epsilon\sigma}c_{1\epsilon\sigma} - c^{\dagger}_{1\theta\sigma}c_{1\theta\sigma}\right) - \left(c^{\dagger}_{2\epsilon\sigma}c_{2\epsilon\sigma} - c^{\dagger}_{2\theta\sigma}c_{2\theta\sigma}\right)\right], \tag{34}$$

$$\Phi = \sum_{k,\gamma,\gamma'}\Delta_k(\gamma,\gamma')c_{k\gamma'\downarrow}c_{k\gamma\uparrow}, \tag{35}$$

where the operator $c_{k\gamma\sigma}$ is defined as

$$c_{k\gamma\sigma} = \frac{1}{\sqrt{2}}\left(c_{1\gamma\sigma} + e^{ik}c_{2\gamma\sigma}\right), \tag{36}$$

where k is either 0 or π,[2] and Δ_k is a complex parameter to be determined variationally under the normalization and the antisymmetric conditions

$$\sum_{k,\gamma,\gamma'} |\Delta_k(\gamma,\gamma')|^2 = 1 \text{ and } \Delta_k(\gamma,\gamma') = \Delta_k(\gamma',\gamma). \tag{37}$$

With using the operator A^c, we can define the charge response function as

$$\chi^c(\omega) = -\mathrm{i}\int_0^\infty \mathrm{d}t\, \mathrm{e}^{\mathrm{i}\omega t - 0^+ t} \langle [A^c(t), A^c(0)] \rangle . \tag{38}$$

Similarly, we can define other response functions χ^s and χ^o in terms of A^s and A^o, respectively. We can also define the pairing response function by

$$\chi^p(\omega) = -\mathrm{i}\int_0^\infty \mathrm{d}t\, \mathrm{e}^{\mathrm{i}\omega t - 0^+ t} \langle [\Phi(t), \Phi^\dagger(0)] \rangle . \tag{39}$$

In calculating $\chi^p(\omega)$ at $\omega \to 0^+$ (static limit), we optimize the parameters $\Delta_k(\gamma,\gamma')$ so as to maximize the absolute value of $\chi^p(0)$, through which we can automatically determine a favorable types of electron pairing for given set of parameters U', J, and g. More specifically, we can find the better pairing between the two possibilities; one is the pairing with their total electronic pseudospin $T = 0$ (SCP0) and the other is the pairing with $T = 1$ (SCP1). We denote the former by χ^{p0} and the latter by χ^{p1}.

The response functions in the noninteracting two-site four-electron system are easily calculated to give $\chi^c(0) = \chi^s(0) = \chi^o(0) = 2\chi^p(0) = -1/t$. We shall normalize the static response functions by the corresponding values in the noninteracting system; $\tilde{\chi} \equiv -t\chi(0)$ for A^c, A^s, and A^o, while $\tilde{\chi} \equiv -2t\chi(0)$ for Φ.

Now we shall show our calculated results along the line I in Fig. 8. For the sake of convenience, let us divide the values of J into three regions; weak-coupling ($0 \lesssim J/t \lesssim 0.5$), intermediate-coupling ($0.5 \lesssim J/t \lesssim 1$), and strong-coupling ($J/t \gtrsim 1$). The ground-state and the first-excited-state energies are shown in Fig. 9. In the entire region of the phase diagram, the ground state is always characterized by $S = T = 0$. In the weak-coupling region where the effect of g dominates that of J, the electrons form an intra-site singlet state and the first-excited state is specified by $S = 0$ and $T = 1$, suggesting the dominance of orbital fluctuations. In the intermediate-coupling region, on the other hand, the electrons begin to form spin-triplet states at both sites due to the Hund's-rule coupling, but S remains to be zero

[2] Note that we define k modulo 2π, indicating that $-k = k$.

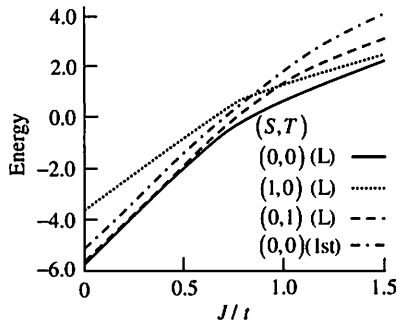

Fig. 9 Ground-state and first-excited-state energies in units of ω_0 of the two-site four-electron $E \otimes e$ system for $t = \omega_0$, $g = \omega_0$, and $J/U' = 0.5$. S and T denote the total spin and pseudospin of the system, respectively. Solid curve ((0, 0) (L)) indicates the lowest energy in the sector with $(S, T) = (0, 0)$ sector; dotted curve ((1, 0) (L)) the lowest energy in the sector with $(S, T) = (1, 0)$; *dashed curve* ((0, 1) (L)) the lowest energy in the sector with $(S, T) = (0, 1)$; *dashed-dotted curve* ((0, 0) (1st)) the first-excited-state energy in the sector with $(S, T) = (0, 0)$

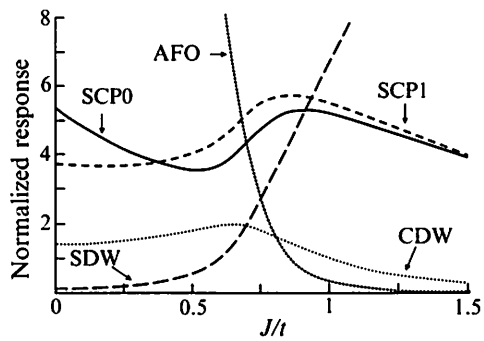

Fig. 10 The normalized response functions for $t = \omega_0$, $g = \omega_0$, and $J/U' = 0.5$. SCP0 is the response of the singlet Cooper pairing with pseudospin zero ($\tilde{\chi}^{p0}$), SCP1 that of the singlet Cooper pairing with pseudospin one ($\tilde{\chi}^{p1}$), AFO the antiferro-orbital ordering ($\tilde{\chi}^{o}$), SDW ($\tilde{\chi}^{s}$), and CDW ($\tilde{\chi}^{c}$). Note that the results for SCP0, SCP1, and CDW are given in ten times magnification

brought about by the electron hopping term or the superexchange antiferromagnetic interaction. From this viewpoint, this phase should be regard as a inter-site singlet state rather than a local-triplet state. Finally in the strong-coupling region, the first-excited state changes into the one with $S = 1$, implying the dominance of spin fluctuations.

The results for the response functions are plotted in Fig. 10 in which a sharp crossover and the concomitant enhancement of SCP0 and SCP1 are seen. (The total number of excited phonons in the system was cut off at sixteen, which is enough for convergence.)

In the weak-coupling region, the AFO response is largest, as expected from the result of $T = 1$ for the first-excited state (see Fig. 9) and the electrons form local singlet states with either the total-pseudospin-zero state (P0) described by

$(d^\dagger_{j\alpha\uparrow}d^\dagger_{j\beta\downarrow} - d^\dagger_{j\alpha\downarrow}d^\dagger_{j\beta\uparrow})/\sqrt{2}$ or the total-pseudospin-one state (P1) described by either $d^\dagger_{j\alpha\uparrow}d^\dagger_{j\alpha\downarrow}$ or $d^\dagger_{j\beta\uparrow}d^\dagger_{j\beta\downarrow}$. The weight of the P0 state is larger than that of the P1 state, leading to the larger response in SCP0 than that in SCP1. As J is gradually turning on, both AFO and SCP response functions begin to decrease, reflecting the gradual breaking of the local singlet pairing.

In the intermediate-coupling region, SCP0 and SCP1 cease to decrease and then increase; each has a peak in the vicinity of the crossover from AFO to SDW states. This enhancement corresponds to the growth of the inter-site pairing, as seen by inspecting the forms for P0 and P1. In this region, P0 is represented by either $(d^\dagger_{1\alpha\uparrow}d^\dagger_{2\beta\downarrow} - d^\dagger_{1\alpha\downarrow}d^\dagger_{2\beta\uparrow})/\sqrt{2}$ or $(d^\dagger_{1\beta\uparrow}d^\dagger_{2\alpha\downarrow} - d^\dagger_{1\beta\downarrow}d^\dagger_{2\alpha\uparrow})/\sqrt{2}$, while P1 by either $(d^\dagger_{1\alpha\uparrow}d^\dagger_{2\alpha\downarrow} - d^\dagger_{1\alpha\downarrow}d^\dagger_{2\alpha\uparrow})/\sqrt{2}$ or $(d^\dagger_{1\beta\uparrow}d^\dagger_{2\beta\downarrow} - d^\dagger_{1\beta\downarrow}d^\dagger_{2\beta\uparrow})/\sqrt{2}$. Then the diagonal hopping makes SCP1 dominate over SCP0.

In the strong-coupling region, the SDW response dominates, as expected from the result of $S = 1$ for the first-excited state (see Fig. 9). The decrease of the SCP0 and SCP1 responses can be understand in terms of the Lehmann representation of χ^{p} as

$$\lim_{\omega\to 0}\chi^{\mathrm{p}}(\omega) = -\sum_n \frac{|\langle 2,n|\Phi|\mathrm{G}\rangle|^2 + |\langle 6,n|\Phi^\dagger|\mathrm{G}\rangle|^2}{E(2,n) + 2\mu - E_{\mathrm{G}}}, \tag{40}$$

where $|\mathrm{G}\rangle$ is the ground state, $|N,n\rangle$ denotes the nth excited state of the N-electron system, $E(N,n)$ is its energy. (In deriving (40), we have exploited particle-hole symmetry.) In the two-electron system, each electron becomes localized at a different site as J increases, leading to the saturation of the ground-state energy $E(2,0)$, but the situation is different in the four-electron system; E_{G} does not saturate but increases almost linearly with $U' - J$. Thus the energy denominator $E(2,n) + 2\mu - E_{\mathrm{G}}$ becomes large as J and U' increase with keeping J/U' fixed, resulting in the decrease of the SCP0 and SCP1 responses. Physically, the period of antiferromagnetic order is comparable to the coherence length of the spin-singlet Cooper pair and these two orders do not coexist in this situation.

We have also explored the situation in which g is increased with other parameters kept fixed. The qualitative behaviors of the response functions are almost the same as those along the line I, except for the sharpness of the crossover, as illustrated in Fig. 11 for the number of excited phonons associated with each electron.

4.3 Two-Band Hubbard Model with Hund's-rule coupling

Inspired by fullerene superconductors, Capone et al. [68] studied a two-band (or two-orbital) Hubbard model, defined by the Hamiltonian H described as

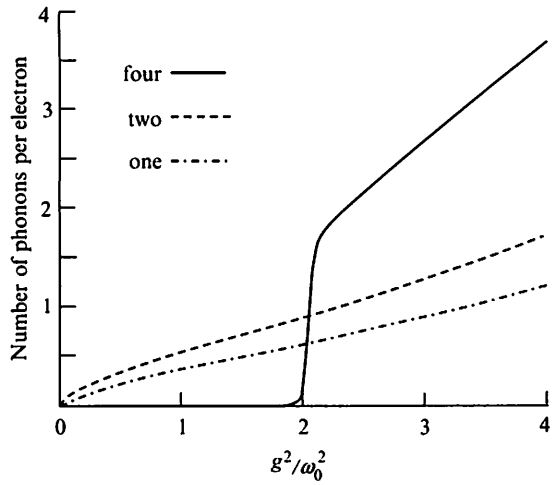

Fig. 11 The number of phonons per electron of the two-site $E \otimes e$ system for $t = \omega_0$, $U' = 3\omega_0$, and $J = 1.5\omega_0$. The *solid curve* (four) represents the result for the four-electron system, the *dashed curve* (two) for the singlet two-electron system, and the *dashed-dotted* curve (one) for the single-electron system. (We have achieved convergence by cutting off the total number of excited phonons at thirty-two in this four-electron system)

$$H = -t \sum_{(\mathrm{j},\mathrm{j}')} \sum_{\gamma\sigma} \left(d^{\dagger}_{\mathrm{j}\gamma\sigma} d_{\mathrm{j}'\gamma\sigma} + d^{\dagger}_{\mathrm{j}'\gamma\sigma} d_{\mathrm{j}\gamma\sigma} \right) + \frac{\bar{U}}{2} \sum_{\mathrm{j}} n_{\mathrm{j}}(n_{\mathrm{j}} - 1) + 2\bar{J} \sum_{\mathrm{j}\sigma\sigma'} d^{\dagger}_{\mathrm{j}\alpha\sigma} d^{\dagger}_{\mathrm{j}\beta\sigma'} d_{\mathrm{j}\alpha\sigma'} d_{\mathrm{j}\beta\sigma}, \tag{41}$$

with $\bar{U} \geq 0$ and $\bar{J} \leq 0$. Note that (1) the sign of $\bar{J}$ is *negative*, and (2) this Hamiltonian can be regarded as an effective Hamiltonian for the $E \otimes e$ molecular-crystal model in the anti-adiabatic and *weak-coupling* regime of g, but the effect of g dominates over the Hund's-rule coupling. The ground state of this model was analyzed around half-filling by means of DMFT. Since the electrons locally form a singlet state due to the inverted Hund's-rule coupling, this system goes to a *local-singlet Mott insulator* in the limit of $\bar{U} \to \infty$ at half-filling. Attention was paid to the physics near this Mott transition.

Using DMFT, Capone et al. calculated the s-wave superconducting gap Δ as a function of $\bar{U}$ and obtained an intriguing ground-state phase diagram in the $(\bar{U}/W, \delta)$ space, shown in Fig. 12, where δ is the doping concentration. It is remarkable that in the very weak-coupling region of $\bar{J}$ ($|\bar{J}|/W = 0.05$ with W the bare bandwidth), $\bar{U}$ enhances the Cooper pairing close to the Mott transition ($\bar{U}/W \sim 0.8$), as called *the strongly correlated superconductivity* (SCS). Another DMFT analysis by Han [110], based on the $E \otimes e$ molecular crystal model without the usual Hund's-rule coupling, supported the emergence of this SCS.

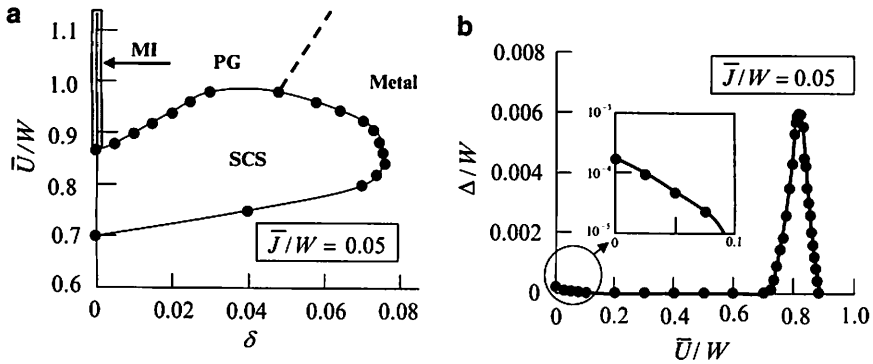

Fig. 12 (**a**) Ground-state phase diagram for the model with inverted Hund's-rule coupling with δ the doping concentration. (**b**) Superconducting gap at half filling as a function of $\bar{U}/W$ [112]. MI, PG, and SCS indicate Mott insulating, pseudogap, and strongly-correlated superconducting phases, respectively

The scenario leading to SCS is explained as follows: In the Hamiltonian (41), there are two interactions, $\bar{U}$ and $\bar{J}$. $\bar{J}$ is an attraction responsible for the Cooper pairing, while $\bar{U}$ is a repulsive interaction to renormalize W into the narrower effective bandwidth W^*, which is given by $W^* = zW$ with z the renormalization factor. Since $\bar{J}$ is not anticipated to be renormalized by $\bar{U}$ [67], the ratio $|\bar{J}|/W^*$ becomes larger as $\bar{U}$ increases. As is suggested by studies on the attractive Hubbard model [111], Δ may become large, if the effective bandwidth and the attraction become comparable, leading to the peak structure in Δ as a function of $\bar{U}$ for $|\bar{J}|/W^* \sim 1$.

In real systems, the effectively negative $\bar{J}$ inevitably indicates the rather strong $g_{E\otimes e}$ in competition with the bare Coulombic orbital-exchange interaction J. Then, as shown in Fig. 11, there would appear the effects of $g_{E\otimes e}$ that are not included in the simple reduction leading to $\bar{J}$. Study of the $E\otimes e$ JT system with fully including the dynamic phonon effects and faithfully treating the Hund's-rule coupling is an important challenge.

4.4 Bipolaron Superconductivity

Although the intermediate-coupling region is realistic and most interesting, it is also most difficult to treat accurately. Before considering this difficult problem, it would be helpful to investigate extreme situations of weak- and strong-coupling regions.

In the former region, an electron–phonon interaction brings about an attraction between electrons, leading to superconductivity in the BCS scenario. In this sense, it is a well-explored region. In the strong-coupling region, on the other hand, it is not the case, although the concept of bipolaron superconductivity is

believed to be basically correct. In fact, the scenario of Bose–Einstein condensation (BEC) of many bipolarons is not matured enough, because many issues including the mass enhancement/renormalization and the repulsion between bipolarons are not satisfactorily solved yet. In this subsection, we shall touch on this bipolaron superconductivity.

Let us start with the $A \otimes a$ Holstein model. In the strong-coupling region, it is usually the case to employ the Lang-Firsov transformation [80], defined as

$$\tilde{c}_{j\sigma} = e^{-iS} c_{j\sigma} e^{iS} = e^{\lambda(a_j - a_j^\dagger)} c_{j\sigma}, \text{ and } \tilde{a}_j = e^{-iS} a_j e^{iS} = a_j - \lambda n_j, \tag{42}$$

where $\lambda = g_{A\otimes a}/\omega_0$ and

$$S = i\lambda \sum_j n_j \left(a_j - a_j^\dagger\right). \tag{43}$$

Then the original Holstein Hamiltonian H_H is rewritten with these new variables by

$$\begin{aligned} H_H = &-t \sum_{\langle j,j'\rangle\sigma} \left(c_{j\sigma}^\dagger c_{j'\sigma} + c_{j'\sigma}^\dagger c_{j\sigma}\right) + \omega_0 \sum_j \tilde{a}_j^\dagger \tilde{a}_j \\ &- 2\lambda^2 \omega_0 \sum_j \tilde{n}_{j\uparrow} \tilde{n}_{j\downarrow} - (\mu + \lambda^2 \omega_0) \sum_j \tilde{n}_j. \end{aligned} \tag{44}$$

Treating the first two terms in the right hand side of (44) within second-order perturbation, we obtain

$$H_{\text{eff}} = -\tilde{t} \sum_{\langle j,j'\rangle} \left(B_j^\dagger B_{j'} + B_{j'}^\dagger B_j\right) + 2\tilde{V} \sum_{\langle j,j'\rangle} \rho_j \rho_{j'} - 2\tilde{\mu} \sum_j \rho_j, \tag{45}$$

where the the quasi-boson operator $B_j^\dagger$ and its density operator ρ_j are defined as

$$B_j^\dagger = \tilde{c}_{j\uparrow}^\dagger \tilde{c}_{j\downarrow}, \text{ and } \rho_j = \tilde{n}_{j\sigma} = \frac{1}{2}\tilde{n}_j, \tag{46}$$

respectively. The various parameters in (44) have been defined by

$$\tilde{t} = \frac{2t^2}{\omega_0} e^{-2\lambda^2} \sum_{nm} \frac{(-1)^{n+m}}{n!m!} \frac{\lambda^{2(n+m)}}{n+m+2\lambda^2}, \tag{47}$$

$$\tilde{V} = \frac{2t^2}{\omega_0} e^{-2\lambda^2} \sum_{nm} \frac{1}{n!m!} \frac{\lambda^{2(n+m)}}{n+m+2\lambda^2}, \tag{48}$$

$$\tilde{\mu} = \mu + 2\lambda^2 \omega_0 + \frac{1}{2} z \tilde{V}, \tag{49}$$

where z is the coordination number.

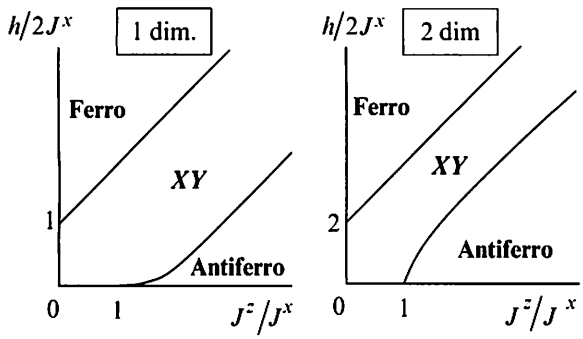

Fig. 13 Schematic ground-state phase diagram for the spin-1/2 XXZ model in the magnetic field in one [115] and two dimensions [119]. The line of $h = 0$ corresponds to the half-filling in the Holstein model. Antiferromagnetic, ferromagnetic, and XY phases correspond, respectively, to charge density wave, band insulating, and superconducting states in the Holstein model

Now, by exploiting the similarity of the commutation relations of $[B_j, B_{j'}^\dagger] = (1 - 2\rho_j)\delta_{jj'}$ and $[S_j^-, S_{j'}^+] = -2S_j^z\delta_{jj'}$, we can introduce *the exact mapping* of the operators $B_j^\dagger$ and ρ_j to the spin 1/2 operators through

$$B_j^\dagger \to S_j^+, \text{ and } \rho_j \to S_j^z + 1/2. \tag{50}$$

With this exact mapping, we can transform H_H to the Hamiltonian H_{XXZ} representing the spin-1/2 quantum XXZ model [113, 114], written by

$$H_{XXZ} = 2\sum_{(jj')}\left(J^x S_j^x S_{j'}^x + J^y S_j^y S_{j'}^y + J^z S_j^z S_{j'}^z\right) - h\sum_j S_j^z, \tag{51}$$

where the parameters J^x, J^y, J^z, and h are, respectively, defined by[3]

$$J^x = J^y = \tilde{t}, J^z = \tilde{V}, \text{ and } h = 2\mu + 4\lambda^2\omega_0. \tag{52}$$

The spin-1/2 XXZ model has been extensively investigated, especially for the case of one dimension by both the Bethe–ansatz approach [115] and field-theoretic methods [116]. In Fig. 13, the ground-state phase diagram is shown in the $(h/2J^x, J^z/J^x)$ space. In the regions specified by "Ferro" and "Antiferro", the ground state is characterized by a finite energy gap excitation, indicating that the corresponding state in the mapped Holstein system is an insulator. More specifically, the former corresponds to a band insulating state, while the latter to a CDW phase. In the region indicated by "XY", the gapless ground state appears, implying the

[3] The sign of J^x can be changed by a canonical transformation without changing those of h and J^z, and is not essential. The ratios of J^z/J^x and h/J^x are relevant.

appearance of a conducting state. According to Leggett [117], the conducting phase in a pure Bose system is assumed to be always superfluid at zero temperature.

In two dimensions, the ground-state phase diagram has been obtained by quantum Monte Carlo simulation [118, 119]. There is a little difference in the vicinity of the Heisenberg point ($J^x = J^z$) from that in one dimension, but they are qualitatively quite similar.

The XXZ model is equivalent to a hard-core Bose–Hubbard model with only nearest-neighbor hopping and interaction. Recently the Bose–Hubbard model has been investigated, but exact phase diagrams have not been obtained so far in three or larger dimensions. It is hoped that DMFT will clarify the phase diagram in infinite dimensions.

Finally we consider the JT bipolarons. In the original $E \otimes e$ model, two vibrational modes are doubly-degenerate. Instead, we treat the $E \otimes (b_1 + b_2)$ model, the Hamiltonian of which reads

$$H = -\sum_{(\mathrm{j},\mathrm{j}')}\sum_{\sigma\gamma\gamma'} t_{\gamma\gamma'}\left(c^{\dagger}_{\mathrm{j}\gamma\sigma}c_{\mathrm{j}'\gamma'\sigma} + c^{\dagger}_{\mathrm{j}'\gamma'\sigma}c_{\mathrm{j}\gamma\sigma}\right) - \mu\sum_{\mathrm{j}} n_{\mathrm{j}} + \sum_{\mathrm{j}}\sum_{l=1,2}\omega_l a^{\dagger}_{\mathrm{j}l}a_{\mathrm{j}l}$$
$$+ g_1\sum_{\mathrm{j}}\left(n_{\mathrm{j}\alpha} - n_{\mathrm{j}\beta}\right)\left(a_{\mathrm{j}1} + a^{\dagger}_{\mathrm{j}1}\right) + g_2\sum_{\mathrm{j}\sigma}\left(c^{\dagger}_{\mathrm{j}\alpha\sigma}c_{\mathrm{j}\beta\sigma} + c^{\dagger}_{\mathrm{j}\beta\sigma}c_{\mathrm{j}\alpha\sigma}\right)\left(a_{\mathrm{j}2} + a^{\dagger}_{\mathrm{j}2}\right). \tag{53}$$

When $g_1 = g_2$ and $\omega_1 = \omega_2$, this model is reduced to the $E \otimes e$ JT system. For simplicity, we assume that $g_1/\omega_1 \gg g_2/\omega_2$ and treat the g_2 term within second-order perturbation. By adopting a similar method in treating the Holstein model, we can map the $E \otimes (b_1 + b_2)$ model into the effective spin model as

$$H = 2\sum_{(\mathrm{j},\mathrm{j}')}\sum_{\gamma\gamma'}\sum_{p} J^{p}_{\gamma\gamma'}S^{p}_{\mathrm{j}\gamma}S^{p}_{\mathrm{j}'\gamma'} + 2\sum_{\mathrm{j}p} J^{p}_{\perp}S^{p}_{\mathrm{j}\alpha}S^{p}_{\mathrm{j}\beta} - h\sum_{\mathrm{j}\gamma} S^{z}_{\mathrm{j}\gamma}, \tag{54}$$

where $h = 2\mu$ and other parameters are given as

$$J^{x}_{\gamma\gamma'} = J^{y}_{\gamma\gamma'} = \frac{2t^2_{\gamma\gamma'}}{\omega_1}e^{-2\lambda_1^2}\sum_{nm}\frac{(-1)^{n+m}}{n!m!}\frac{\lambda_1^{2(n+m)}}{n+m+2\lambda_1^2}, \tag{55}$$

$$J^{z}_{\gamma\gamma'} = \frac{2t^2_{\gamma\gamma'}}{\omega_1}e^{-2\lambda_1^2}\sum_{nm}\frac{1}{n!m!}\frac{\lambda_1^{2(n+m)}}{n+m+2\lambda_1^2}, \tag{56}$$

$$J^{x}_{\perp} = J^{y}_{\perp} = \frac{2g_2^2}{\omega_1}e^{-4\lambda_1^2}\sum_{n}\frac{1}{n!}\frac{(-1)^n(2\lambda_1)^{2n}}{n+2\lambda_1^2+\omega_2/\omega_1}, \tag{57}$$

$$J^{z}_{\perp} = 4\lambda_1^2\omega_1 + \frac{2g_2^2}{\omega_1}e^{-4\lambda_1^2}\sum_{n}\frac{1}{n!}\frac{(2\lambda)^{2n}}{n+2\lambda_1^2+\omega_2/\omega_1}. \tag{58}$$

Note (1) there are two kinds of spins S_α and S_β per site and (2) $J^z_\perp$ is much larger than the other interaction parameters.

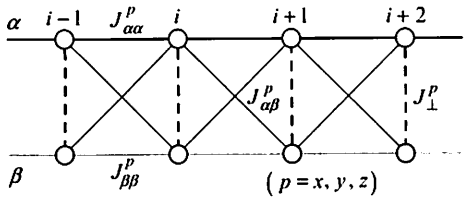

Fig. 14 Schematic representation of the effective spin model for the $E \otimes (b_1 + b_2)$ molecular crystal system in one dimension. $J^p_{\gamma\gamma'}$ $(\gamma, \gamma' = \alpha, \beta; p = x, y, z)$ denotes the interaction between nearest-neighbor spins γ and γ'. $J^p_{\perp}$ is the on-site interaction between α and β at the same site

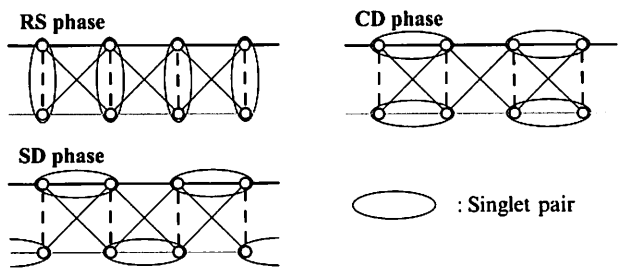

Fig. 15 Schematic pictures for three phases that may exist in the relevant parameter region at half-filling. RS denotes rung singlet, CD columnar dimerization, and SD staggered dimerization, respectively. There may be other possible phases

In one dimension, this spin model is represented by a two-leg ladder system [120] as shown in Fig. 14 and examples of possible phases are schematically given in Fig. 15. In two dimensions, we may think of the effective spin model as shown in Fig. 16. As we see, those spin models are the subject of intense researches in relation to HTSC and at present we cannot give a further reliable information.

5 Conclusions and Future Prospects

We have reviewed the recent developments in the field of the Jahn–Teller effect on itinerant electrons in Jahn–Teller crystals. In Sect. 1, we have summarized the current status of the researches on the fullerene superconductors and the manganite perovskites exhibiting the colossal magnetoresistance and concluded that, although various impressive findings have been made in relation to those oxides, there still remain many challenging problems, reflecting the intrinsic complexities of those materials. In Sect. 2–4, we have focused on the model JT systems, in particular, the canonical $E \otimes e$ model, and discussed some of the interesting features of polarons and bipolarons in the JT crystals, including our own original contributions.

In concluding this review, we have to admit that the researches on the JT effect on itinerant electrons are still in a very early stage, considering the richness of the

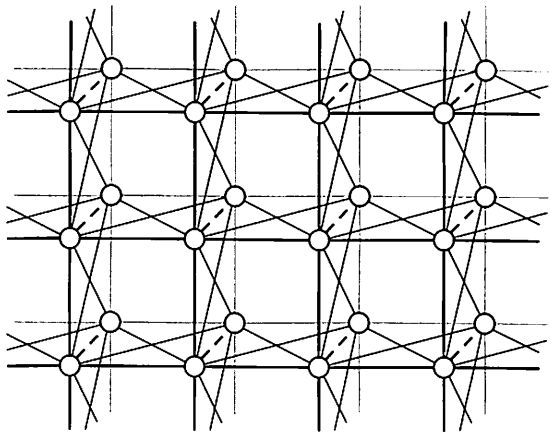

Fig. 16 Schematic representation of the effective spin model for the $E \otimes (b_1 + b_2)$ molecular crystal system in two dimensions. The two-leg ladders, each of which represents a one-dimensional $E \otimes (b_1 + b_2)$ crystal, are piled in the direction of z axis

problem concerning the interplay among spin, charge, orbital, and phonon degrees of freedom. We would presume that this field of research will pose very good challenging projects for the next-generation supercomputers and hope that such heavy numerical works will open a new rich field of physics and chemistry.

Acknowledgements This work was partially supported by Global COE Program "the Physical Sciences Frontier", the Ministry of Education, Culture, Sports, Science, and Technology (MEXT), Japan as well as by a Grant-in-Aid for Scientific Research in Priority Areas "Development of New Quantum Simulators and Quantum Design" (No.17064004) of MEXT, Japan. We would like to thank M. Kaplan, H. Koizumi, T. Hotta, and H. Maebashi for useful discussions for years.

References

1. H.A. Jahn, E. Teller, Proc. R. Soc. Lond. **A161**, 220 (1937)
2. R. Engleman, *The Jahn–Teller Effect in Molecules and Crystals* (Wiley, New York, 1972)
3. I.B. Bersuker, *The Jahn–Teller Effect* (Cambridge University Press, Cambridge, 2006)
4. M.D. Kaplan, B.G. Vekhter, *Cooperative Phenomena in Jahn–Teller Crystals* (Plenum, New York, 1995)
5. J.G. Bednorz, K.A. Müller, Z. Phys. B **64**, 189 (1986)
6. A.F. Hebard, M.J. Rosseinsky, R.C. Haddon, D.W. Murphy, S.H. Glarum, T.T.M. Palstra, A.P. Ramirez, A.R. Kortan, Nature **350**, 600 (1991)
7. S. Jin, T.H. Tiefel, M. McCormack, R.A. Fastnacht, R. Ramesh, J.H. Chen, Science **264**, 413 (1994)
8. Y. Tokura, Y. Tomioka, H. Kuwabara, A. Asamitsu, Y. Moritomo, M. Kasai, J. Appl. Phys. **79** 5288 (1996)
9. C. Zener, Phys. Rev. **82** 403 (1951)
10. P.W. Anderson, H. Hasegawa, Phys. Rev. **100**, 675 (1955)
11. P.-G. de Gennes, Phys. Rev. **118** 141 (1960)

12. A.J. Millis, P.B. Littlewood, B.I. Shariman, Phys. Rev. Lett. **74** 5144 (1995)
13. N. Mannella, A. Rosenhahn, C.H. Booth, S. Marchesini, B.S. Mun, S.-H. Yang, K. Ibrahim, Y. Tomioka, C.S. Fadley, Phys. Rev. Lett. **92** 166401 (2004)
14. Z. Popovic, S. Satpathy, Phys. Rev. Lett. **84** 1603 (2000)
15. C. Ederer, C. Lin, A.J. Millis, Phys. Rev. B **76** 155105 (2007)
16. A.P. Ramirez, J. Phys. : Condens. Matter **9**, 8171 (1997)
17. A. Mareo, S. Yunoki, E. Dagotto, Science **283** 2034 (1999)
18. Y. Tokura, in *Colossal Magnetoresistive Oxides*, ed. by Y. Tokura (Gordon & Breach, Amsterdam, 2000)
19. Y. Tokura, N. Nagaosa, Science **288** 462 (2000)
20. E. Dagotto, T. Hotta, A. Moreo, Phys. Rep. **344** 1 (2001)
21. M.B. Salamon, M. Jaime, Rev. Mod. Phys. **73** 583 (2001)
22. Y. Takada, T. Hotta, Int. J. Mod. Phys. B **15** 4267 (2001)
23. J. van den Brink, D. Khomskii, Phys. Rev. B **63** 140416(R) (2001)
24. T. Hotta, Y. Takada, H. Koizumi, Int. J. Mod. Phys. B **12** 3437 (1998)
25. T. Hotta, Y. Takada, H. Koizumi, E. Dagotto, Phys. Rev. Lett. **84** 2477 (2000)
26. Y. Takada, T. Hotta, H. Koizumi, Int. J. Mod. Phys. B **13** 3778 (1999)
27. T. Holstein, Ann. Phys. **8** 325 (1959)
28. C.M. Varma, J. Zaanen, K. Raghavachari, Science **254** 989 (1991)
29. M. Schluter, M. Lannoo, M. Needels, G.A. Baraff, D. Tomanek, Phys. Rev. Lett. **68** 526 (1992)
30. I.I. Mazin, S.N. Rashkeev, V.P. Antropov, O. Jepsen, A.I. Liechtenstein, O.K. Andersen, Phys. Rev. B. **45** 5114 (1992)
31. S. Suzuki, K. Nakao, Phys. Rev. B. **52** 14206 (1995)
32. A.P. Ramirez, Superconduct. Rev. **1** 1 (1994)
33. M.P. Gelfand, Superconductivity Review **1** 103 (1994)
34. O. Gunnarsson, Rev. Mod. Phys. **69** 575 (1997)
35. L. Degiorgi, Adv. Phys. **47** 207 (1998)
36. Y. Takada, T. Hotta, Int. J. Mod. Phys. B **12** 3042 (1998)
37. B. Sundqvist, Adv. Phys. **48** 1 (1999)
38. S. Suzuki, S. Okada, K. Nakao, J. Phys. Soc. Jpn. **69** 2615 (2000)
39. O. Gunnarsson, *Alkali-Doped Fullerides* (World Scientific, Singapore, 2004)
40. T.W. Ebbesen, J.S. Tsai, K. Tanigaki, J. Tabuchi, Y. Shimakawa, Y. Kubo, I. Hirosawa, J. Mizuki, Nature **355** 620 (1992)
41. A.P. Ramirez, A.R. Kortan, M.J. Rosseinsky, S.J. Duclos, A.M. Mujsce, R.C. Haddon, D.W. Murphy, A.V. Makhija, S.M. Zahurak, K.B. Lyons, Phys. Rev. Lett. **68** 1058 (1992)
42. A.A. Zakhidov, K. Imaeda, D.M. Petty, K. Yakushi, H. Inokuchi, K. Kikuchi, I. Ikemoto, S. Suzuki, Y. Achiba, Phys. Lett. A **164** 355 (1992)
43. C.-C. Chen, C.M. Lieber, J. Am. Chem. Soc. **114**, 3141 (1992)
44. W.L. McMillan, Phys. Rev. **167** 331 (1968)
45. P.B. Allen, R.C. Dynes, Phys. Rev. B **12** 905 (1975)
46. T. Yildirim, J.E. Fischer, R. Dinnebier, P.W. Stephens, C.L. Lin, Solid State Commun. **93** 269 (1995)
47. G.M. Eliashberg, Sov. Phys. JETP **11** 696 (1960)
48. A.B. Migdal, Sov. Phys. JETP **7** 996 (1958)
49. Y. Takada, J. Phys. Chem. Solids **54** 1779 (1993)
50. O. Gunnarsson, G. Zwicknagl, Phys. Rev. Lett. **69** 957 (1992)
51. N. Manini, E. Tosatti, A. Auerbach, Phys. Rev. B **49** 13008 (1994)
52. L.F. Chibotaru, A. Ceulemans, Phys. Rev. B **53** 15522 (1996)
53. C.C. Chancey, M.C.M. OfBrien, *The Jahn–Teller Effect in C_{60} and Other Icosahedral Complexes* (Princeton University Press, Princeton, 1997)
54. S. Wehrli, M. Sigrist, Phys. Rev. B **76** 125419 (2007)
55. Y. Wang, R. Yamachika, A. Wachowiak, M. Grobis, M.F. Crommie, Nat. Mater. **7** 194 (2008)
56. D.M. Deaven, D.S. Rokhsar, Phys. Rev. B **48** 4114 (1993)
57. C.-C. Chen, C.M. Lieber, Science **259** 655 (1993)

58. M. Riccò, F. Gianferrari, D. Pontiroli, M. Belli, C. Bucci, T. Shiroka, Europhys. Lett. **81** 57002 (2008)
59. A. Georges, G. Kotliar, W. Krauth, M.J. Rozenberg, Rev. Mod. Phys. **68** 13 (1996)
60. J.E. Han, O. Gunnarsson, V.H. Crespi, Phys. Rev. Lett. **90** 167006 (2003)
61. T. Yildirim, L. Barbedette, J.E. Fischer, C.L. Lin, J. Robert, P. Petit, T.T.M. Plastra, Phys. Rev. Lett. **77** 167 (1996)
62. E. Cappelluti, P. Paci, C. Grimaldi, L. Pietronero1, Phys. Rev. B **72**, 054521 (2005)
63. Y. Takada, Physica C **364-365** 71 (2001)
64. J.E. Han, E. Koch, O. Gunnarsson, Phys. Rev. Lett. **84** 1276 (2000)
65. J.E. Han, O. Gunnarsson, Phys. B **292** 196 (2000)
66. Y. Iwasa, H. Shimoda, T.T.M. Palstra, Y. Maniwa, O. Zhou, T. Mitani, Phys. Rev. B **53** R8836 (1996)
67. M. Capone, M. Fabrizio, C. Castellani, E. Tosatti, Science **296** 2364 (2002)
68. M. Capone, M. Fabrizio, C. Castellani, E. Tosatti, Phys. Rev. Lett. **93** 047001 (2004)
69. K. Tanigaki, I. Hirosawa, T.W. Ebbesen, J. Mizuki, J.S. Tsai, J. Phys. Chem. Solids **54** 1645 (1993)
70. Y. Takada, Int. J. Mod. Phys. B **21** 3138 (2007)
71. Y. Takada, J. Phys. Soc. Jpn. **65** 3134 (1996)
72. Y. Takada, J. Phys. Soc. Jpn. **65** 1544 (1996)
73. M.R. Schafroth, S.T. Butler, J.M. Blatt, Helv. Phys. Acta **30** 93 (1957)
74. J.M. Blatt *Theory of Superconductivity* (Academic, New York, 1964)
75. A.S. Alexandrov, J. Ranninger, Phys. Rev. B **23** 1796 (1981)
76. A.S. Alexandrov, J. Ranninger, Phys. Rev. B **24** 1164 (1981)
77. Y. Takada, Phys. Rev. B **26** 1223 (1982)
78. A.S. Alexandrov, N.F. Mott, *Polarons and Bipolarons* (World Scientific, Singapore, 1995)
79. D.R. Pooler, J. Phys. A: Math. Gen. **11** 1045 (1978)
80. I.G. Lang, Yu. A . Firsov, Sov. Phys. JETP **16** 1301 (1963)
81. T.D. Lee, F.E. Low, D. Pines, Phys. Rev. **90** 297 (1953)
82. H. Fröhlich, Phys. Rev. **79** 845 (1950)
83. P.E. Kornilovitch, Phys. Rev. Lett. **81** 5382 (1998)
84. E. Jeckelmann, S.R. White, Phys. Rev. B **57** 6376 (1998)
85. J. Bonča, S.A. Trugman, I. Batistič, Phys. Rev. B **60** 1633 (1999)
86. J. Bonča, T. Katrašnik, S.A. Trugman, Phys. Rev. Lett. **84** 3153 (2000)
87. S. Ciuchi, F. de Pasquale, S. Fratini, D. Feinberg, Phys. Rev. B **56**, 4494 (1997)
88. A.S. Mishchenko, N.V. Prokof'ev, A. Sakamoto, B.V. Svistunov, Phys. Rev. B. **62** 6317 (2000)
89. A.S. Alexandrov (Ed.), *Polarons in Advanced Materials*: Springer series in materials science **103** (Canopus Publishing and Springer Gmbh, Bath, UK, 2007).
90. H. Fehske, R. Schneider, A. Weiße (Eds.), *Computational Many-Particle Physics* (Springer, Heidelberg, 2008)
91. K. -H. Höck, H. Nickisch, H. Thomas, Helv. Phys. Acta **56** 237 (1983)
92. K. Ziegler, Phys. Rev. B **72** 075120 (2005)
93. Y. Takada, Phys. Rev. B **61** 8631 (2000)
94. P.E. Kornilovitch, Phys. Rev. Lett. **84** 1551 (2000)
95. H. Barentzen, Eur. Phys. J. B **24** 197 (2001)
96. S. El Shawish, J. Bonča, L.-C. Ku, S.A. Trugman, Phys. Rev. B **67**, 014301 (2003).
97. S.A. Trugman, L.-C. Ku, J. Bonča, J. Supercond. **17**, 193 (2004)
98. R. Ramakumar, S. Yarlagadda, Phys. Rev. B **69** 104519 (2004)
99. H. Barentzen, J. Phys.: Condes. Matter **17** 4713 (2005)
100. Y. Takada, M. Masaki, J. Mol. Struct. **838** 207 (2007)
101. Y. Takada, M. Masaki, J. Supercond. Nov. Magn. **20** 629 (2007)
102. H.C. Longuet-Higgins, U. ÖPik, M.H.L. Pryce, R.A. Sack, Proc. R. Soc. Lond. **A244** 1 (1958)
103. W. Moffitt, W. Thorson, Phys. Rev. **108** 1251 (1957)
104. M.C.M. O'Brien, J. Phys. A: Math. Gen. **22** 1779 (1989)
105. Y.M. Liu, C.A. Bates, J.L. Dunn, V.Z. Polinger, J. Phys.: Condens. Matter **8** L523 (1996)

106. T. Okuda, A. Asamitsu, Y. Tomioka, T. Kimura, Y. Taguchi, Y. Tokura, Phys. Rev. Lett. **81** 3203 (1998)
107. A. Macridin, G.A. Sawatzky, M. Jarrell, Phys. Rev. B **69**, 245111 (2004)
108. J.E. Han, O. Gunnarsson, Phys. B **292** 196 (2000)
109. M. Fabrizio, E. Tosatti, Phys. Rev. B **55** 13465 (1997)
110. J.E. Han, Phys. Rev. B **70** 054513 (2004)
111. R. Micnas, J. Ranninger, S. Robaszkiewicz, Rev. Mod. Phys. **62** 113 (1990)
112. M. Schiró, M. Capone, M. Fabrizio, C. Castellani, Phys. Rev. B **77** 104522 (2008)
113. J.E. Hirsch, E. Fradkin, Phys. Rev. B **27**, 4302 (1983)
114. J.K. Freericks, Phys. Rev. B **48** 3881 (1993)
115. M. Takahashi, *Thermodynamics of One-dimensional Solvable Models* (Cambridge University Press, Cambridge, 1999)
116. D.C. Cabra, P. Pujol, in *Quantum Magnetism*, ed. by U. Schollwöck, J. Richter, D.J.J. Farnell, R.F. Bishop. Lect. Notes Phys. **645** (Springer, Heidelberg, 2004), p. 253
117. A.J. Leggett, Phys. Fenn. **8** 125 (1973)
118. F. Hébert, G.G. Batrouni, R.T. Scalettar, G. Schmid, M. Troyer, A. Dorneich, Phys. Rev. B, **65**, 014513 (2001)
119. G. Schmid, S. Todo, M. Troyer, A. Dorneih, Phys. Rev. Lett. **88**, 167208 (2002).
120. G.-H. Liu, H.-L. Wang, G.-S. Tian, Phys. Rev. B **77**, 214418 (2008) and references therein

Index